(12) INTERNATIONAL APPLICATION PUBLISHED UNDER THE PATENT COOPERATION TREATY (PCT)

(19) World Intellectual Property Organization
International Bureau

(43) International Publication Date
01 February 2018 (01.02.2018)

WIPO | PCT

(10) International Publication Number
WO 2018/022983 A1

(51) International Patent Classification:
H01M 4/36 (2006.01) *H01M 4/58* (2010.01)
H01M 4/42 (2006.01) *H01M 4/38* (2006.01)
H01M 4/02 (2006.01) *H01M 4/48* (2010.01)
H01M 4/44 (2006.01)

(21) International Application Number:
PCT/US2017/044351

(22) International Filing Date:
28 July 2017 (28.07.2017)

(25) Filing Language: English

(26) Publication Language: English

(30) Priority Data:
62/368,231 29 July 2016 (29.07.2016) US

(71) Applicants: **MASSACHUSETTS INSTITUTE OF TECHNOLOGY** [US/US]; 77 Massachusetts Avenue, Cambridge, Massachusetts 02139 (US). **NATIONAL UNIVERSITY OF SINGAPORE** [SG/SG]; 21 Lower Kent Ridge Road, 119077 (SG).

(72) Inventors: **PEREGO, Daniele**; c/o Singapore-MIT Alliance for Research and Technology Centre, 1 CREATE Way, #10-01 CREATE Tower, 138602 (SG). **OMAMPULIYUR SWAMINATHAN, Rajamouly**; 635 Pasir Ris Drive 1, #04-598, 510635 (SG). **THU, Ye Lin**; c/o Singapore-MIT Alliance for Research and Technology Centre, 1 CREATE Way, #10-01 CREATE Tower, 138602 (SG). **SHAO-HORN, Yang**; c/o Massachusetts Institute of Technology, 77 Massachusetts Avenue, Cambridge, Massachusetts 02139 (US).

(72) Inventor: **KIONG, Choi Wee** *(deceased)*.

(72) Inventor: **THOMPSON III, Carl Vernette**; c/o Massachusetts Institute of Technology, 77 Massachusetts Avenue, Cambridge, Massachusetts 02139 (US).

(74) Agent: **KOENIG, III, C. Frederick**; Volpe and Koenig, P.C., United Plaza, Suite 1800, 30 S. 17th Street, Philadelphia, Pennsylvania 19103 (US).

(81) Designated States *(unless otherwise indicated, for every kind of national protection available)*: AE, AG, AL, AM, AO, AT, AU, AZ, BA, BB, BG, BH, BN, BR, BW, BY, BZ, CA, CH, CL, CN, CO, CR, CU, CZ, DE, DJ, DK, DM, DO,

(54) Title: A LI-ION THIN FILM MICROBATTERY AND METHOD OF FABRICATING THE SAME

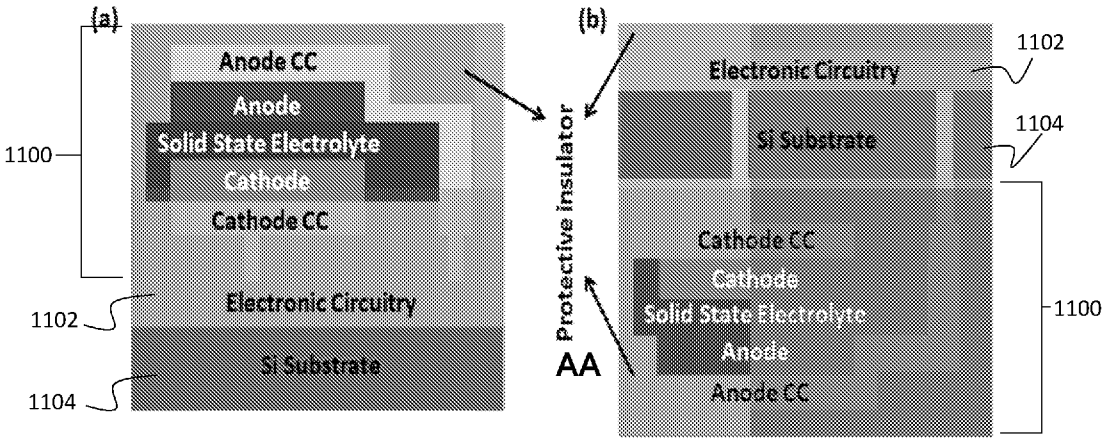


Figure 11

(57) Abstract: A Li-ion thin film microbattery, a microbattery array, a method of fabricating a Li-ion thin film microbattery and a method of fabricating a microbattery array. The Li-ion thin film microbattery comprises a Li-free cathode comprising a transition metal oxide thin film; an anode comprising a lithiated Ge or Si thin film; and an electrolyte film disposed between the cathode and the anode; wherein a Li-source of the Li-ion thin film microbattery is provided by means of the lithiated Ge or Si thin film.

[Continued on next page]

WO 2018/022983 A1

DZ, EC, EE, EG, ES, FI, GB, GD, GE, GH, GM, GT, HN, HR, HU, ID, IL, IN, IR, IS, JO, JP, KE, KG, KH, KN, KP, KR, KW, KZ, LA, LC, LK, LR, LS, LU, LY, MA, MD, ME, MG, MK, MN, MW, MX, MY, MZ, NA, NG, NI, NO, NZ, OM, PA, PE, PG, PH, PL, PT, QA, RO, RS, RU, RW, SA, SC, SD, SE, SG, SK, SL, SM, ST, SV, SY, TH, TJ, TM, TN, TR, TT, TZ, UA, UG, US, UZ, VC, VN, ZA, ZM, ZW.

(84) **Designated States** *(unless otherwise indicated, for every kind of regional protection available)*: ARIPO (BW, GH, GM, KE, LR, LS, MW, MZ, NA, RW, SD, SL, ST, SZ, TZ, UG, ZM, ZW), Eurasian (AM, AZ, BY, KG, KZ, RU, TJ, TM), European (AL, AT, BE, BG, CH, CY, CZ, DE, DK, EE, ES, FI, FR, GB, GR, HR, HU, IE, IS, IT, LT, LU, LV, MC, MK, MT, NL, NO, PL, PT, RO, RS, SE, SI, SK, SM, TR), OAPI (BF, BJ, CF, CG, CI, CM, GA, GN, GQ, GW, KM, ML, MR, NE, SN, TD, TG).

Published:

— *with international search report (Art. 21(3))*

A LI-ION THIN FILM MICROBATTERY AND METHOD OF FABRICATING THE SAME

CROSS-REFERENCE TO RELATED APPLICATION

[0001] This application claims the benefit of priority of USA Provisional Application No. 62/368,231 filed on July 29, 2016, the content of which is incorporated herein by reference in its entirety for all purposes.

TECHNICAL FIELD

[0002] This invention relates broadly to a Li-ion thin film microbattery and method of fabricating the same, and to a microbattery array and a method of fabricating the same.

BACKGROUND

[0003] Technological advances in microelectronics have reduced the power requirements of electronic circuitry and micro- electro-mechanical systems, enabling the use of on-chip Li-ion thin film microbatteries for applications such as environmental sensing [1,2], RFID [3]. smart cards [4], Internet of Things (IoT) [5], and even micro-spacecraft [6]. Many more applications can be made possible when microbatteries are directly integrated with electronic circuitry rather than placed separately on a printed circuit board (PCB).

[0004] Microbatteries can be fabricated using thin film technologies commonly used for manufacture of other microsystems [7,8]. Li-ion thin film microbatteries (TFMs) typically include a cathode comprising a Li-containing transition metal oxide or the like, an anode typically made by Lithium metal and a solid electrolyte made by Lithium Phosphorus Oxynitride (LiPON).

[0005] In order to meet the increasing demands on capacity and performance, new concepts for Li-ion microbatteries that can be manufactured in a simple manner are desirable. The critical issues inhibiting the large-scale commercial adoption of Li-ion microbatteries to-date are: (i) relatively low capacity of Li-containing cathode materials; (ii) safety concerns when using pure Li metal as the anode; (iii) reduced reliability when using high capacity anode (Si); and (iv) integrability with CMOS processes and platforms.

[0006] Embodiments of the present invention seek to address one or more of the above-mentioned needs.

SUMMARY

[0007] In accordance with a first aspect of the present invention there is provided a Li-ion thin film microbattery comprising a Li-free cathode comprising a transition metal oxide thin film; an anode comprising a lithiated Ge or Si thin film; and an electrolyte film disposed between the cathode and the anode; wherein a Li-source of the Li-ion thin film microbattery is provided by means of the lithiated Ge or Si thin film.

[0008] In accordance with a second aspect of the present invention there is provided a microbattery array comprising two or more of the Li-ion thin film microbattery of the first aspect.

[0009] In accordance with a third aspect of the present invention there is provided a method of fabricating a Li-ion thin film microbattery, comprising the steps of providing a Li-free cathode comprising a transition metal oxide thin film; providing an anode comprising a lithiated Ge or Si thin film; and providing an electrolyte film disposed between the cathode and the anode; wherein a Li-source of the Li-ion thin film microbattery is provided by means of the lithiated Ge or Si thin film

[0010] In accordance with a fourth aspect of the present invention there is provided a method of fabricating a microbattery array, comprising fabricating two or more Li-ion thin film microbatteries using the method of the third aspect.

BRIEF DESCRIPTION OF THE DRAWINGS

[0011] The invention will be better understood with reference to the detailed description when considered in conjunction with the non-limiting examples and the accompanying drawings, in which:

[0012] Figure 1 shows a graph illustrating output voltage vs. volumetric specific capacity of RuO_2 thin film for use in example embodiments deposited in Ar and O_2 plasma environment.

[0013] Figure 2 shows a graph illustrating comparative Ge vs Si areal specific capacity, for use in example embodiments.

[0014] Figure 3(a) shows a field emission scanning electron microscopy (FE-SEM) top-view and cross-section (insert) images of an as-deposited RuO_x thin film sputter deposited using a pure O_2 plasma, for use in example embodiments.

[0015] Figure 3(b) shows a transmission electron microscopy (TEM) bright-field cross-section image and a selected area electron diffraction pattern (SAEDP) (insert) in a RuO_x thin film deposited using a pure O_2 plasma, for use in example embodiments.

[0016] Figure 4(a) shows cyclic voltammograms obtained at a scan rate 0.5 mV/s in 300nm RuO_x | $LiPF_6$ | Li cells, with Li metal also used as a reference electrode, specifically 1st-cycle for an as-deposited RuO_x film sputter deposited using pure argon and pure oxygen, respectively, for use in example embodiments.

[0017] Figure 4(b) shows cyclic voltammograms obtained at a scan rate 0.5 mV/s in 300nm RuO_x | $LiPF_6$ | Li cells, with Li metal also used as a reference electrode, specifically 3rd cycle for sputter deposited RuOx films made using pure argon and pure oxygen, respectively, for use in example embodiments.

[0018] Figure 5(a) shows charge/discharge profiles for RuO_x films (300nm RuO_x | $LiPF_6$ | Li) characterized at a rate of 0.1C at room temperature, voltage window: 0.75-3.5 V vs. Li/Li^+, for use in example embodiments.

[0019] Figure 5 (b) shows a graph illustrating capacity retention for RuO_x thin films at room temperature for use in example embodiments, the films sputter deposited using different Ar/O_2 gas mixtures.

[0020] Figure 6 shows a graph illustrating volumetric specific capacity of RuO_x thin films as a function of oxygen atomic stoichiometry, for use in example embodiments.

[0021] Figure 7(a) shows a graph illustrating in-situ stress evolution of Ge anode for use in an example embodiment, during lithiation/delithiation.

[0022] Figure 7(b) shows a graph illustrating in-situ stress evolution of Si anode for use in an example embodiment, during lithiation/delithiation.

[0023] Figure 8 shows a graph illustrating rate performance of Si and Ge anodes for use in example embodiments.

[0024] Figure 9(a) shows a schematic drawing illustrating bi-layer sputtered pre-lithiated anode for use in an example embodiment.

[0025] Figure 9(b) shows a schematic drawing illustrating multi-layer sputtered pre-lithiated anode for use in an example embodiment.

[0026] Figure 9(c) shows a schematic drawing illustrating co- sputtered pre-lithiated anode for use in an example embodiment.

[0027] Figure 10(a) shows a schematic drawing illustrating microbattery integration with electronic circuitry through wafer-bonding according to an example embodiment, specifically electronic circuitry on Si substrate.

[0028] Figure 10(b) shows a schematic drawing illustrating microbattery integration with electronic circuitry through wafer-bonding according to an example embodiment, specifically microbattery on Si substrate.

[0029] Figure 10(c) shows a schematic drawing illustrating microbattery integration with electronic circuitry through wafer-bonding according to an example embodiment, specifically integrated stack.

[0030] Figure 11(a) shows a schematic drawing illustrating direct deposition of microbattery according to an example embodiment, specifically microbattery on top of electronic circuitry.

[0031] Figure 11(b) shows a schematic drawing illustrating direct deposition of microbattery according to an example embodiment, specifically microbattery on the back of the Si substrate.

[0032] Figure 12(a) shows a schematic drawing illustrating a microbattery array according to an example embodiment, specifically a top-view schematic.

[0033] Figure 12(b) shows a schematic drawing illustrating a microbattery array according to an example embodiment, specifically cross-section of a single microbattery of the microbattery array.

[0034] Figure 12(c) shows an equivalent circuit of a microbattery array according to an example embodiment.

[0035] Figure 13 shows a plot showing electrochemical performance of a proof-of-concept CMOS-integrable microbattery prototype example embodiment based on RuO_2 cathode, LiPON electrolyte, pre-lithiated Si anode.

[0036] Figure 14 a) shows a graph illustrating Si areal capacity as a function of charge/discharge cycle at different rate for different Si thicknesses, for use in example embodiments.

[0037] Figure 14 b) shows a graph illustrating Si relative areal capacity normalized to first charge/discharge cycle at different rate for different Si thicknesses, for use in example embodiments.

[0038] Figure 15 a) shows a graph illustrating Si/LiPON areal capacity as a function of charge/discharge cycle at different rate for different Si thicknesses, for use in example embodiments.

[0039] Figure 15 b) shows a graph illustrating Si/LiPON relative areal capacity normalized to first charge/discharge cycle at different rate for different Si thicknesses, for use in example embodiments.

[0040] Figure 16 a) shows graph illustrating Ge areal capacity as a function of charge/discharge cycle at different rate for different Ge thicknesses, for use in example embodiments.

[0041] Figure 16 b) shows a graph illustrating Ge relative areal capacity normalized to first charge/discharge cycle at different rate for different Ge thicknesses, for use in example embodiments.

[0042] Fig. 17 a) shows a graph illustrating Ge/LiPON areal capacity as a function of charge/discharge cycle at different rate for different Ge thicknesses, for use in example embodiments.

[0043] Figure 17 b) shows a graph illustrating Ge/LiPON relative areal capacity normalized to first charge/discharge cycle at different rate for different Si thicknesses, for use in example embodiments.

[0044] Figure 18 shows a flow chart illustrating a method of fabricating a Li-ion thin film microbattery, according to an example embodiment.

DETAILED DESCRIPTION

[0045] Example embodiment of the present invention can provide for a Li-ion thin film microbattery that can be easily integrated into microelectronic or other microsystems fabrication processes.

[0046] Example embodiment of the present invention can provide for a high capacity cathode material (Li-free transition metal oxides such as V_2O_5, CrO_3, RuO_2) implementation into Li-ion microbatteries.

[0047] Example embodiment of the present invention can provide for a high capacity, improved cyclability and safety anode material (Si and Ge) implementation into Li-ion microbatteries.

[0048] Example embodiment of the present invention can provide for Li-source implementation (in the anode side) into Li-ion microbatteries (referred as pre-lithiation technique).

[0049] Example embodiment of the present invention can also provide new design and process fabrication for integrable Li-ion thin film microbattery arrays characterized by customizable output power and improved reliability.

[0050] In energy storage field, one of the key parameters widely used to compare different electrode active materials is gravimetric specific capacity measured by [mAh/g] or [Ah/Kg] metrics. However, microbatteries are restricted in terms of the amount of areal footprint the microbattery stack can occupy. Therefore, the areal specific capacity of electrodes is a far more important metric measured by [mAh/cm^2] or [$\mu Ah/cm^2$] units. Moreover, since areal specific capacity is a function of the volumetric specific capacity, the key parameter in the Li-ion thin film microbatteries field is the volumetric specific capacity measured by rescaling the areal specific capacity over the thickness of the electrode [$mAh/cm^2\mu m$] or [$\mu Ah/cm^2\mu m$].

[0051] Considering the volumetric specific capacity a list of possible cathode materials can be found in Table 1. Among them it is possible to identify two different classes: the first one made by cathodes containing Li in their stoichiometry while the second one is characterized by Li-free transition metal oxides cathode materials.

Cathode materials	Volumetric specific capacity [μAh/cm^{2}μm]
$LiCoO_2$	63.7
$LiNiO_2$	62.1
$LiMnO_2$	64.5
$LiNi_{0.5}Mn_{0.5}O_2$	65.1
$LiMn_2O_4$	63.3
$LiFePO_4$	61.2
$LiMnPO_4$	73.7
CrO_3	434.2
V_2O_5	147.8
RuO_2	561.8

Table 1. Cathode material volumetric specific capacities [9]

[0052] The increasing demand on capacity might be solved by introducing Li-free transition metal oxide cathodes such as CrO_3, V_2O_5 and RuO_2 that are characterized by a very high volumetric specific capacity. A drawback of such cathodes is the absence of Li-ions within their structure, which makes them unusable in current state-of-the-art Li-ion microbatteries, where cathodes act as the Li-ion source. Indeed the state-of-the-art for Li-ion thin film microbattery cathode is typically restricted to LiM_xO_y stoichiometries where M is a transition metal such as Co, Mn, Ni or a mixture of transition metals). Li containing cathode materials act as the Li-source for the full microbattery, and in the first charge cycle the Li is transferred to the anode materials. The advantages of this family of materials are (i) good cyclability, (ii) safety, and (iii) reasonable rate performance. However, as a class, these materials have limited volumetric specific capacity for storage of Li (the highest is $LiNi_{0.5}Mn_{0.5}O_2$ ~ 65.1 μAh/cm^{2}μm). To this stage the overall energy capacity of a microbattery is generally limited by the capacity of the cathode, as higher capacity anode materials are available and implemented.

[0053] In example embodiments of the present invention, Li-free transition metal oxides are instead implemented as cathode active materials for Li-ion thin film microbatteries. For example RuO_2 is characterized by a very high volumetric specific capacity [561.8 $\mu Ah/cm^2\mu m$], due to its ability to incorporate up to 4mol Li atoms per mol of RuO_2 during the discharge phase via the following reaction:

[0054] $RuO_2 + 4e^- + 4Li^+ \rightarrow Ru + 2Li_2O$

[0055] RuO_2 thin film can be deposited through a variety of techniques such as, but not limited to: chemical vapor deposition, electrodeposition, physical vapor deposition. In example embodiments sputtering deposition of a RuO_2 target in Ar, O_2 and a mixture Ar:O_2 plasma environment is used. Electrochemical performance of as synthesized RuO_2 thin film in Ar (curves 100) and O_2 (curves 102) are shown in Figure 1.

[0056] RuO_2 can provide an overall volumetric specific energy of about 1014,2 $mWh/cm^2\mu m$, which is 5 times greater with respect to the state-of-the-art $LiCoO_2$ volumetric specific energy (248,5 $mWh/cm^2\mu m$). While Li-free transition metal oxide cathodes have a relatively large voltage dispersion as a function of charge state (i.e. the absence of a voltage plateau), with respect to state-of-the-art ($LiCoO_2$ and $LiFePO_4$), this can preferably be addressed in example embodiments by developing an integrated/CMOS compatible fabrication process and/or the fabrication of a Li-ion thin film microbatteries array, as will be described in more detail below. The output voltage and power can be appropriately fine-tuned in example embodiment by integrating the microbattery with a suitable CMOS driver circuit such as amplifiers and/or by coupling different Li-ion thin film microbatteries in an array.

[0057] *Substrate preparation for transition metal oxide, such as, but not limited to, RuO_x thin films for use in example embodiments*

[0058] RuO_x thin films were deposited on several types of substrates, including stainless steel (SS) discs, and Ti/Pd layers deposited on SiO_2-coated Si wafers. Deposition of RuO_x layers on Ti/Pd films on oxidized Si wafers were well suited for scanning electron microscopy (SEM), transmission electron microscopy (TEM) and x-ray diffraction (XRD) characterization. Electrochemical performance was investigated using SS discs, which acted both as current collectors and non-reactive substrates. SS discs of 1.2 cm in diameter and 0.5 mm in thickness were cut from an AISI 316 L sheet and mechanically polished to create a mirror-like smooth surface, avoiding roughness effects on the electrochemical

characterization. The mechanical polishing involved three different steps: (i) use of P800 (3M Imperial Sandpaper) SiC polishing paper, (ii) followed by P1600 (3M Imperial Sandpaper) SiC polishing paper and (iii) finally a 0.1 μm Al_2O_3 powder dispersion. Sonication in DI water and acetone was used to remove organic and inorganic compounds from the SS surface.

[0059] *Synthesis of RuO_x thin films for use in example embodiments*

[0060] RuO_x thin films were deposited using sputter deposition from a stoichiometric RuO_2 target (3 inch, 99,995% purity, ALB Materials) in an RF magnetron sputtering system (ANELVA®) at room temperature with an Ar/O_2 plasma. The target was pre-sputtered at 50 W for 10 minutes, which was followed by deposition for five hours at the same power. During the deposition, the sample stage was rotated at 40 rpm to ensure uniform deposition. The background pressure was in the range $\sim 2\times10^{-6}$ Torr. The flow rates of Ar and O_2 were adjusted to vary the composition of Ar and O_2 in the mixed plasma (Table 2). Depositions were carried out at 4.00 mPa.

[0061] *Characterization of RuO_x thin films for use in example embodiments*

[0062] All samples were weighed before and after sputter deposition using a RADWAG-MYA/2Y microbalance (resolution: 0.001 mg) to determine the mass of the deposited RuO_x. Surface morphologies and cross-sections were observed using a field-emission scanning electron microscope (FE-SEM, FEI Inspect F50) equipped with an Energy Dispersive X-ray spectrometer (EDX, Oxford PentaFET) used for chemical analysis (performed at 10 KeV).

[0063] The crystal structure of the sample was characterized using X-ray diffraction (XRD, Bruker D8 Advance) with Cu $K\alpha_1$ radiation at a scan rate of 1° min^{-1} for 2Ø between 20 and 90 (both powder diffraction and single crystal XRD were carried out), as well as high-resolution selected area electron diffraction (SAED) using a JEOL 2100F transmission electron microscope (TEM) operating at 200 keV. Cross-sectional samples were prepared for TEM characterization by depositing 50 nm of carbon and 150 nm of platinum followed by ion milling using a focus ion beam in a system also equipped for scanning electron microscopy (FEI Nova 600i Nanolab).

[0064] *Electrochemical measurements of RuO_x thin films for use in example embodiments*

[0065] Electrochemical tests were conducted in a half-cell setup using a tom cell. Half-cells consisting of as-prepared RuO_x cathodes, lithium metal anodes and lithium reference electrodes were characterized using a 1 M $LiPF_6$ in ethylene carbonate/diethyl carbonate (V/V = 1:1) electrolyte, and a Celgard poly-propylene separator. Cells were assembled in an Ar-filled glove box with H_2O and O_2 levels less than 0.1 ppm. Investigations of the electrochemical performance were performed outside the glove box at room temperature. Cyclic Voltammetry (CV) and galvanostatic cycling were carried out from 0.75 to 3.6 V with respect to the Li/Li^+ electrode using a BioLogic VMP3 station and NEWARE High Precision Battery Testing System. The charge and discharge cycles refer to the lithiation and delithiation of the RuO_x electrode, respectively. Charge/discharge cycles were performed at a current density of 30 $\mu A/cm^2$ (corresponding to ~75 mA/g, ~0.1C).

[0066] *Results and discussion of RuO_x thin films for use in example embodiments*

[0067] Figure 3 (a) shows FE-SEM top-view and cross-section (insert) images of an as-deposited RuO_x thin film. A columnar structure was detected in the cross-sectional image while the top surface was found to be relatively smooth. The surface morphology of the thin film was not affected by the Ar/O_2 plasma composition. TEM analysis of an RuO_x thin film deposited using a pure O_2 plasma showed a columnar structure (Figure 3 (b)) and selected area diffraction patterns (SAEDP), Figure 3 (b-insert), showed that the as-deposited RuO_x thin film had a polycrystalline nanostructure.

[0068] Cross-sectional SEM images were used to evaluate thin film thickness, which, in turn, was used to evaluate the specific volumetric capacity. Thickness measurements also allow determination of an average growth rate under different plasma conditions (Table 2). As the O_2 mole fraction in the plasma was increased, the total mass and thickness of the deposited material decreased. The calculated mass density and growth rate decreased accordingly, from 9.18 to 6.17 g/cm^3 and from 2.6 to 1.2 nm/min, respectively. The density of the as-deposited $RuO_{1.92}$ is slightly lower than the theoretical density of crystalline RuO_2 (6.97 g/cm^3). The differences in the film density shown in Table 2 can be attributed to an increase in the weight percentage of oxygen within the RuO_x films with increasing oxygen partial pressure in the O_2/Ar plasma. This has also been confirmed using EDX and Rutherford backscattering spectrometry (RBS) measurements, which indicated the weight percentage of the different elements in the films (Table 2): the ruthenium-to-oxygen ratio of the films increased with the mole fraction of O_2 in the

sputtering gas. A 26.4 % oxygen plasma (which corresponds to a pO_2 of about ~1.056 mPa) leads to an oxygen content close to the ruthenium oxide stoichiometric value ($RuO_{1.92}$).

O_2 in plasma [%]	Thickness [nm]	Deposited mass [mg]	Calculated density [g/cm^3]	Calculated growth rate [nm/min]	Ruthenium [%]	Oxygen [%]	Oxygen stoichiometry
0	769 ± 11	0.798 ± 0.002	9.18	2.56	83.7	16.3 ± 1.4	1.23
18.2	659 ± 6	0.582 ± 0.001	7.81	2.20	79.2	20.8 ± 0.8	1.66
26.4	593 ± 5	0.449 ± 0.011	6.70	1.98	76.7	23.3 ± 2.2	1.92
50.0	468 ± 5	0.370 ± 0.003	6.99	1.56	72.5	27.5 ± 1.5	2.39
100	360 ± 6	0.251 ± 0.003	6.17	1.20	72.0	28.0 ± 3.6	2.46

Table 2. Physical characteristics and EDX analysis of as-deposited RuO_x thin films.

[0069] Figure 4 (a) shows cyclic voltammetry results for the first charge-discharge cycle in the voltage range 0.75-3.6 V for RuO_x films deposited using pure Ar and pure O_2 plasmas. During the first lithiation, for RuO_x grown in Ar (curve 400), three peaks are observed at 0.90, 1.21 and 1.51 V, indicating a multi-step lithiation process. As reported elsewhere [29-31], the experimental observations are consistent with a two-step mechanism for lithium insertion, the first of which is a simple intercalation of lithium ions in the RuO_2 crystal lattice, forming a orthorhombic $LiRuO_2$ structure, followed by conversion at higher capacities into nanocrystalline Li_2O and Ru nano-/amorphous phases [30]. In contrast, RuO_x films deposited with pure oxygen (curve 402) show a single CV peak at 0.80 V (Figure 4 (a)). In the first delithiation, RuO_x films deposited using pure Ar showed three peaks at 1.30, 2.16 and 2.65 V, which are similar to the values observed during the first delithiation of RuO_x films deposited using a pure O_2 plasma (1.30, 2.15 and 2.66 V). From the second CV cycle onwards, both Ar plasma (curve 404) and O_2 plasma (curve 406) samples exhibit two lithiation peaks (1.15 and 0.90 V) and four delithiation peaks (1.33, 2.16, 2.68 and 3.17 V), see Figure 4(b). That these voltages are similar in both sets of samples after the first lithiation, suggests that the lithiation/delithiation mechanisms are the same after the first cycle.

[0070] Figure 5 shows the cycling behavior of RuO_x films deposited with different Ar/O_2 ratios. First-cycle charge/discharge profiles (Figure 5 (a)) show regions of reduced slope at similar potentials across all samples, curves 501-505 (1.75 and 0.9 V during discharge and 1.3, 2.1, 2.7 V during charge). Increasing the oxygen partial pressure during deposition led to films with higher oxygen contents and to enhanced capacities, showing a higher volumetric capacity (0.55 $mAh/cm^2\mu m$) for 100% O_2 than films deposited using a pure Argon plasma (0.32 $mAh/cm^2\mu m$). The capacity increase can be attributed to the increased availability of oxygen for formation of Li_2O during lithiation of the electrode [29-31. In addition, the cycling stability was increased significantly when O_2 was introduced in the sputtering gas, see curves 511 to 515 in Figure 5(b). After 50 cycles at 0.1 C, the RuO_x film deposited using a pure O_2 plasma can still deliver a capacity of 425.6 $\mu Ah/cm^2\mu m$, indicating a capacity retention of 77.01 %, compared to 176.55 $\mu Ah/cm^2\mu m$ with a retention of 54.76 % for films deposited using a pure Ar plasma. During the delithiation phase of charge/discharge cycles, high tensile stresses develop within the RuO_x thin films, due to repeated volume expansion/contraction. As previously reported by Zhu et al. [32-33], this can lead to crack formation and propagation of microcracks, resulting in a subsequent pulverization and delamination of the film from the current collector.

[0071] RuO_x films can provide an overall volumetric energy of about 1014.2 $mWh/cm^2\mu m$, which is 5 times greater than that of $LiCoO_2$ films volumetric specific energy (~248.5 $mWh/cm^2\mu m$). Considering only active material, our results for both specific capacity and energy density are in good agreement with previous results given by Kim et al. [29] for RuO_2 powders. That the high capacity of RuO_x electrodes can be obtained in as-deposited thin films demonstrates their great potential for use in high performance TFMs

[0072] While RuO_x films can exhibit a relatively large voltage variation as a function of the state of charge (i.e. the absence of a voltage plateaus), compared to materials such as $LiCoO_2$ and $LiFePO_4$, for TFMs, this limitation can be overcome by developing an integrated control circuit. Electronic circuits typically require a stable (constant voltage) and clean (low noise) power supply voltage as many parameters that define their performance depend on the supply voltage. In general, any battery is only partially able to supply a sufficiently stable clean voltage because its output voltage reduces and its output impedance increases as the energy capacity diminishes, and its output voltage dips when a

large current is drawn. To circumvent these limitations, a power management circuit is routinely employed embodying a DC-DC converter [34-37] to provide a stable supply voltage from a poorly defined output battery voltage - a Boost DC-DC converter [37] to step-up (increase) the output voltage or Buck DC-DC [34] to step-down (reduce) the output voltage. If a very stable or low-noise output voltage is required, a Low-DropOut (LDO) voltage regulator is applied to the output of the DC-DC converter. In general both the DC-DC converter and LDO feature low output impedance. In other words, power management can be employed to provide a stable and clean supply voltage despite the high variation in the voltage supplied by a RuO_x-based thin film microbattery according to example embodiments.

[0073] The stoichiometry of the films was found to depend strongly on the O_2 content of the Ar/O_2 sputtering gas. Use of plasmas with low oxygen contents leads to lower oxygen contents in the films. Experimental results also showed that the Ru to O ratio in the thin film has a significant effect on the electrochemical performance, both the volumetric specific capacity (see curve 600 in Figure 6) and capacity retention. In general, volumetric capacities of RuO_x films were higher at greater oxygen concentrations. Volumetric capacities increased with x and approached a plateau of 0.55 $mAh/cm^2\mu m$ beyond x=2. This value is very close to the very high theoretical reversible capacity of crystalline RuO_2 (0.56 $mAh/cm^2\mu m$), making RuO_x films sputter deposited at room temperature suitable as next generation high-capacity cathode materials in thin film Li-ion microbatteries. Synthesis of high capacity cathode layers using only room temperature processes according to example embodiments makes integration with fabrication of other micro-devices and microsystems, such as integrated circuits, much more feasible, advantageously enabling many novel TFMs applications.

[0074] *High capacity, improved cyclability and safety anodes according to example embodiments*

[0075] In view of e.g. safety issues when using pure Li metal as the anode and the reduced reliability when using high capacity anode (Si), example embodiments advantageously use Ge based anode material for Li-ion thin film microbatteries. In microbatteries traditional anode materials are pure Li and Si thin film. Although Si is known as the material characterized by the highest gravimetric specific capacity (~4.4 Li atoms per Si atom, ~0,83 $mAh/cm^2\mu m$), it suffers from a very high volume expansion

while cycling (~420%). In the thin film forms, this volume expansion leads to a very high stress evolution resulting in a very low cyclability of the electrode.

[0076] The advantages of Ge thin film anodes when used in Li-ion microbatteries according to example embodiments can include: (i) higher reliable areal capacity compared to Si, in spite of Ge having a lower volumetric specific capacity compared to Si; (ii) the rate of charge and discharge for Ge is higher than for Si; (iii) Ge has improved safety compared to pure Li.

[0077] While Ge has a higher volumetric specific capacity than conventional anode materials like carbon, it is only about 90% (~0,74 $mAh/cm^2\mu m$) that of Si. However, it has been recognized by the inventors that volumetric specific capacity is not the only one key parameter to be taken in account: cycle life is also a very important feature of Li-ion microbatteries. Cycle life is defined by the number of charge/discharge cycles that a battery can lasts before starts to reduce visibly (conventionally ~80/85% of the initial capacity) its performance.

[0078] As mentioned above, lithiated Si suffers from a large volume expansion of about 420%, whereas Ge only has a volume expansion of about 270% [10]. It has been recognized by the inventors that this difference in volume expansion causes different reliable areal specific capacities for Si and Ge in the thin film form. From experiments with example embodiments of the present invention, it was found that Ge, curves 200a-c, can cycle well at higher thin film thickness compared to Si, curves 202a-c, as shown in Figure 2. This translates to Ge advantageously having a reliable areal specific capacity of about 330 $\mu Ah/cm^2$ compared to Si's 120 $\mu Ah/cm^2$. This three-fold increase in reliable areal specific capacity of Ge over Si, makes it more preferred Li-ion thin film microbattery anode material. Also shown in Figure 2 is data, curves 204a-c, collected on a 487nm thick Si film covered by 1 μm thick LiPON film according to an example embodiment. As will be described further below with reference to Figures 14 to 17, LiPON film on top of the active material (both Si and Ge), advantageously enhances the life cycle of the underneath material significantly, according to example embodiments.

[0079] In the half-cell configuration (i.e. a configuration with a Ti/Pd current collector and Ge/Si thin film, a solid electrolyte (LiPON), a liquid electrolyte ($LiPF_6$) and a Li foil as a counter electrode), a cycle life of about 42 and 247 cycles for 487 nm Si and 548 nm Ge thickness respectively.

[0080] The reason for the difference in cycling performance between Si and Ge is believed to be evident from comparative in-situ stress evolution studies during lithiation/delithiation. It was found that Ge inelastically deforms at much lower stresses than Si. Ge (see curves 700, 702 in Figure 7 (a) for the 27^{th} and 3^{rd} cycle, respectively) has an absolute stress range of 1.5 GPa and Si (see curves 704, 706 in Figure 7 (b) for the 15^{th} and 3^{rd} cycle, respectively) has an absolute stress range of 2.2 GPa, which corresponds to Si having 47% higher absolute stress than Ge as shown in Figures 7 (a) and (b). Si is therefore more susceptible to fracture and pulverization than Ge during lithiation/delithiation.

[0081] It has been reported that the diffusivity of Li-ions in Ge is 400 times higher than in Si at room temperature [12,13]. Here, Li-ions diffusivity is taken to be a measure of the lithiation and delithiation rates. Enhanced diffusivity of Li-ions in Ge compared to Si, is an added advantage to using Ge as a Li-ion anode, according to example embodiments. This advantageously enhances the rate performance of Ge anodes, curve 800, compared to Si anodes, curve 802 (Figure 8), thereby increasing the rate performance of microbatteries with Ge anodes according to example embodiments.

[0082] Pure Li-metal can be used as a high capacity (~0,206 $mAh/cm^2\mu m$) anode material which also serves as Li-ions source in a microbattery. However, safety concerns limit the use of Li-metal as an anode. Potential Li dendrite formation resulting in a short circuit of electrodes, or exposure of Li-metal (in the event of encapsulation failure) to atmospheric ambient resulting in explosive combustion, make it an unsafe anode to be used in commercial Li-ion batteries. Use of Ge anodes in Li-ion microbatteries according to example embodiments advantageously eliminates the need for having Li in its pure metallic phase. Moreover, the theoretical volumetric capacity of Ge anodes (~0,74 $mAh/cm^2\mu m$) is higher than that of Li metal, resulting in a volumetric capacity advantage of example embodiments of the present invention as well.

[0083] Ge thin-films can be deposited through a variety of techniques such as, but not limited to: chemical vapor deposition [16], electrodeposition [17] and physical vapor deposition [18]. Specifically, Ge anodes can be deposited through sputtering, a physical vapor deposition technique according to an example embodiment. In the following, implementation of Ge thin films in a full microbattery stack according to example embodiments will be described.

[0084] The advantages of using a pre-lithiation technique according to example embodiments described herein can include: (i) it makes possible to use Li-free cathode materials; (ii) it leads to improved cyclability/reliability; (iii) it can provide the ability to tailor the amount of Li incorporation to better manage performance vs. cyclability trade-offs; (iv) it can provide improved safety when compared to the use of pure Li-metal; and (v) it can ensure that the Li is never in the form of metallic Li, thereby arresting any stray motion of Li-ions, advantageously making the microbattery stack CMOS compatible when integrated with electronic circuitry.

[0085] Li-ion thin film microbatteries can be deposited through a variety of techniques such as, but not limited to: the sol-gel method [19], chemical vapor deposition [20], electrodeposition [21], ALD [22] or physical vapor deposition [8]. Sputtering deposition is a physical vapor deposition technique. Several examples of how sputter deposition can be used to create pre-lithiated thin films according to example embodiments are described herein. Similar strategies would apply for other film formation techniques in different embodiments. Pre-lithiation of anodes (such as Si or Ge) can be achieved by at least three different sputtering process: (i) sputtering of a pre-lithiated target, (ii) bi-layer, (iii) co-sputtering or (iv) multi-layer deposition.

[0086] In the sputtering of a pre-lithiated target according to example embodiments, Li is present within the stoichiometric structure of the target material such as Li_xSi_y, Li_xGe_y. The fabrication process of the target material may involve chemical methods, electrochemical methods, solid-state reactions, sol-gel preparations. Optimal Li-loading of the electrode can be achieved by engineering the stoichiometry of the target material.

[0087] In the Bi-layer process (Figure 9(a)) according to one embodiment, Li layer 900 is deposited separately on top of the electrode active material layer 902. Lithiated electrodes according to such embodiments are formed through solid-state chemical reactions due to the high chemical reactivity of Li with the electrode active materials. Optimal Li-loading of the electrodes can be achieved by engineering the electrode thin layer 902 to lithium layer 900 thickness ratio. The substrate temperature and other parameters during deposition can be used to control the reaction between the electrode active material layer 902 and Li layer 900.

[0088] In the Multi-layer process (Figure 9(b)) according to another embodiment, alternating thinner layers (compared to the bi-layer process, Figure 9(a)) of Li 904 and

electrode active material 906 are deposited. When the chemical interaction between Li 904 and the electrode active material 906 is lower, this technique preferably ensures a uniform pre-lithiation. The thickness of each individual layer depends on the ease of chemical interaction between Li 904 and the active material 906. The substrate temperature and other parameters during the deposition can be used to control the reaction between the electrode active material layers 906 and Li layers 904.

[0089] In the Co-sputtering process (Figure 9(c)), Li is sputtered together with the electrode active material in the same sputtering chamber at the same time. This can ensure a uniform mix of Li and the active material through the thickness of the deposited film 908. Optimal Li-loading of the anode can be achieved by engineering the active material to lithium deposition-rate ratio.

[0090] In the three processes described above with reference to Figures 9(a)-(c), an additional post-deposition annealing can be used to enhance the chemical reaction between Li and the electrode active material, thereby resulting in a highly uniform pre-lithiated electrode.

[0091] All the four different sputtering processes described above have been investigated according to example embodiments. Presently, the best results have been achieved following the bi-layer process. However, it is believed that by e.g. using an adequate sputtering tools, which allows several depositions without breaking the vacuum (i.e. without exposing target materials and samples to atmosphere), all the four different sputtering processes described above can result in a complete pre-lithiation electrode synthesis.

[0092] *Design and process fabrication for integrable Li-ion thin film microbatteries and/or arrays according to example embodiments*

[0093] High areal/volumetric specific capacity and microbattery cyclability according to example embodiments can enable complex integrated circuits (ICs) with tight (i.e. CMOS-level) integration between the electronic circuits and the microbatteries. The microbatteries canl preferably have the required energy capacity to power the selected parts of the ICs, and preferably have sufficient reliability to last for the useful life of the ICs. This can advantageously lead to an overall miniaturization of the size of ICs, due to the optimal use of the available areal footprint.

[0094] Additionally, integrable microbattery arrays, when paired with CMOS power management circuits according to example embodiments, can allow for customizable and controllable power output, which would allow the optimal use of a microbattery's stored charge, regardless of its output voltage as a function of its charge state (which would address potential challenges faced by microbatteries with large output voltage variation such as the RuO_2 cathode microbatteries described earlier). Smart integrated power management circuits can also be expected to enhance the reliability of the microbatteries (and therefore the entire IC) due to their ability to properly regulate charging and discharging operations for maximal circuit life and efficiency.

[0095] Integration of Li-ion thin film microbatteries makes a Li-ions barrier layer and the use of a CMOS compatible processes desirable to fabricate the microbattery.

[0096] A critical issue in integrated microbatteries is the possibility of contamination of the electronic circuitry by Li-ions. This can affect the electronic circuitry's operation. To prevent Li-ions diffusion and other possible contamination, the right choice of protective insulators is important. A Li-ion barrier layer of Si_3N_4 (also referred as SiN) and/or SiO_2 thin films are used in example embodiments which can be deposited by several methods such as, but not limited to, chemical vapor deposition, ALD, physical vapor deposition or thermal oxidation. By using a Li-barrier layer it is preferably possible to stop any stray motion of Li-ions, making the microbattery stack CMOS compatible. A protective/passivation/encapsulation layer of the microbattery is also desirable to protect the microbattery from the exposure to atmosphere. A Parylene C thin film as passivation layer deposited by a room-temperature CVD process is used according to an example embodiment, advantageously improving the overall compatibility with CMOS processes.

[0097] CMOS compatible processes to fabricate the microbattery can be classified in two different families: (i) separate fabrication of electronic circuitry and microbatteries on silicon substrates, followed by wafer-bonding; or (ii) direct deposition of the microbattery on the top/bottom of the fabricated electronic circuitry. The techniques and advantages of both these routes according to example embodiments are discussed below.

[0098] Wafer-bonding is an established technology for SOI wafers [23], MEMS [24] and strained-Si [25] fabrication. This technique can also be used to integrate microbatteries with electronic circuitry. In this case, the electronic circuitry 1000 (i.e. one or more electronic circuitry layers) is first fabricated on a Si substrate 1002 with

appropriate protective insulation layers 1004 and vias 1006 for current conduction (Figure 10(a)). The microbattery stack 1008 is separately fabricated on a Si substrate 1010, also with appropriate protective insulation layer 1012 and vias 1014 for current conduction (Figure 10(b)). These two wafers/substrates 1002, 1010 are then wafer-bonded as shown as an example embodiment of an integrated microbattery 1016 in Figure 10(c). The choice of wafer-bonding technique can include [24], but is not limited to: direct bonding, anodic bonding or intermediate layer-bonding. The advantage of the wafer-bonding technique includes that there is no limitation on high temperature annealing processes in the fabrication of the microbattery stack 1008. Electronic circuitry is susceptible to failure and performance degradation when high temperature annealing is conducted post-integration. Microbatteries typically consist of three important thin-film layers: anode, cathode and electrolyte. The performance of individual thin-films might be improved through high-temperature annealing. For instance, $LiCoO_2$ is used as a popular thin-film cathode and to achieve high specific capacity the film has to be annealed at 700 °C [26]. Potential thin-film electrolytes such as LAGP also require annealing at 650 - 800 °C [27] for improved ionic conductivity.

[0099] Microbattery integration through wafer-bonding is believed to be preferred when high temperature annealing processes are essential to the fabrication of the microbattery stack.

[0100] When no annealing is required for the microbattery stack fabrication, the stack can be directly deposited on the electronic circuitry's (i.e. one or more electronic circuitry layers) substrate. One specific example in this case is RuO_2, a Li-ion cathode material. RuO_2 does not require annealing as it interacts with Li-ions chemically to form a new phase, rather than through intercalation ($LiCoO_2$) mechanism which requires that the material be crystalline and therefore generally requires high temperature annealing. An example of a microbattery stack fabricated completely at room temperature is composed by RuO_2 (cathode), LiPON (electrolyte) and pre-lithiated Li_xSi_y (anode) [28]. In this approach, there is no need for wafer-bonding as the entire fabrication takes place on a single Si substrate. The microbattery stack 1100 can be deposited on top of the electronic circuitry 1102 (Figure 11(a)) or alternatively can be deposited on the back side of the Si substrate 1104 (Figure 11(b)). The latter option (Figure 11(b)) has the added advantage of the microbattery stack being separated from the electronic circuitry due to thick Si

substrate in between, limiting interactions due to Li transport/migration out of the microbattery.

[0101] In both integration processes, the thin-films of the microbattery can be deposited through a variety of techniques such as, but not limited to: the sol-gel method [19], chemical vapor deposition [20], electrodeposition [21], atomic layer deposition [22] or physical vapor deposition [8]. Sputtering is a physical vapor deposition technique and unlike chemical vapor deposition does not require complex precursor and ambient chemistries. Also, to deposit patterned microbattery thin-films such as those shown in Figure 10 and Figure 11, shadow masks can be used in conjunction with sputter deposition.

[0102] Integrable microbatteries can be fabricated to include more than one individual battery cell. Figure 12(a) shows a schematic top-view of an example of a microbatteries array with 4 individual cells 1201-1204 (Figure 12(c) shows the equivalent circuit). The array can be designed to suit power requirements. It is desirable to ensure that both the anode and cathode current collectors 1206, 1208, respectively, are at the same level as shown in Figure 12(b).

[0103] Microbattery arrays can have the following advantages: (i) customizable power output, and (ii) improved reliability.

[0104] The amount of current and voltage drawn from the microbattery array can be customized. Using the same active battery materials, different current and voltage performance can be achieved. In the equivalent circuit shown in Figure 12(c), the current and voltage drawn from the array is twice as much as that drawn form an individual cell. Therefore, arrays can power a variety of application using the same active battery materials. When integrated with power management circuitry, the battery array can also be reconfigured on-the-fly to modify voltage and power.

[0105] Additionally, arrays are more reliable compared to individual cells. A single cell might fail due to material failure during operation. As an example, consider when two cells are connected in parallel. Even when one of the cells fails, the same voltage can be drawn albeit at half of the current. To further improve reliability, the battery array can be designed in such a way that the non-functioning cells can be by-passed.

[0106] Figure 13 shows a plot showing electrochemical performance of a proof-of-concept CMOS-integrable microbattery prototype example embodiment based on RuO_2

cathode, LiPON electrolyte, pre-lithiated Si anode. In particular a comparison between the example embodiment and state-of-the-art is reported (Cymbet®). Furthermore, a comparison with theoretical limit of Li-containing transition metal oxide ($LiCoO_2$) is reported ("*state-of-the-art Li-ion thin film microbattery cathode is typically restricted to* LiM_xO_y *stoichiometries where M is a transition metal such as Co, Mn, Ni or a mixture of transitionmetals*"). In particular, curves 1300a-c show the charge capacity, the discharge capacity and the efficiency, respectively, for RuO2|LiPON|pre-lithiated Si, according to an example embodiment. Line 1302 illustrates the theoretic limit of the state of the art based on LiCoO2|LiPON|Li, line 1304 illustrates previous results based on LiCoO2|LiPON|Si, and line 1306 illustrates the highest performance theoretically achievable using LiCoO2 cathode.

[0107] Figure 14 a) shows a graph illustrating Si areal capacity as a function of charge/discharge cycle at different rate (C/4; C/2 and C) for different Si thicknesses (curves 1401-1405). Figure 14 b) shows a graph illustrating Si relative areal capacity normalized to first charge/discharge cycle at different rate (C/4; C/2 and C) for different Si thicknesses (curves 1411-1415). Table 3shows forecasts on cycle life of Si anodes at different thicknesses.

99 nm	177 cycles
204 nm	173 cycles
311 nm	69 cycles
417 nm	57 cycles
487 nm	42 cycles

Table 3

[0108] Figure 15 a) shows a graph illustrating Si/LiPON areal capacity as a function of charge/discharge cycle at different rate (C/4; C/2 and C) for different Si thicknesses (curves 1501-1505). Figure 15 b) shows a graph illustrating Si/LiPON relative areal capacity normalized to first charge/discharge cycle at different rate (C/4; C/2 and C) for different Si thicknesses (curves 1511-1515). Table 4 shows forecasts on cycle life of Si/LiPON anodes at different thickness.

99 nm	303 cycles
204 nm	298 cycles
311 nm	226 cycles
417 nm	83 cycles
487 nm	56 cycles

Table 4

[0109] Figure 16 a) shows graph illustrating Ge areal capacity as a function of charge/discharge cycle at different rate (C/4; C/2 and C) for different Ge thicknesses (curves 1601-1605). Figure 16 b) shows a graph illustrating Ge relative areal capacity normalized to first charge/discharge cycle at different rate (C/4; C/2 and C) for different Ge thicknesses (curves 1611-1615). Table 5 shows forecasts on cycle life of Ge anodes at different thickness.

108 nm	1158 cycles
230 nm	821 cycles
339 nm	928 cycles
444 nm	553 cycles
548 nm	247 cycles

Table 5

[0110] Fig. 17 a) shows a graph illustrating Ge/LiPON areal capacity as a function of charge/discharge cycle at different rate (C/4; C/2 and C) for different Ge thicknesses (curves 1701-1705). Figure 17 b) shows a graph illustrating Ge/LiPON relative areal capacity normalized to first charge/discharge cycle at different rate (C/4; C/2 and C) for different Si thicknesses (curves 1711-1715). Table 6 shows forecasts on cycle life of Ge/LiPON anodes at different thickness.

108 nm	1471 cycles
230 nm	1503 cycles
339 nm	1488 cycles
444 nm	1275 cycles
548 nm	1186 cycles

Table 6

[0111] As can be seen from Figures 14 to 17, advantageously (i) –LiPON coating stabilizes mechanically the underneath layers, preventing the solid-electrolyte interface

(SEI) formation and enhancing the life cycles of the films, according to example embodiments, and (ii) Ge behaves better than Si, according to different embodiments.

[0112] According to one embodiments, a Li-ion thin film microbattery is provided comprising a Li-free cathode comprising a transition metal oxide thin film; an anode comprising a lithiated Ge or Si thin film; and an electrolyte film disposed between the cathode and the anode; wherein a Li-source of the Li-ion thin film microbattery is provided by means of the lithiated Ge or Si thin film.

[0113] The transition metal oxide may comprise V_2O_5, CrO_3, and/or RuO_2. The electrolyte film may comprise LiPON. The Li-ion thin film microbattery may further comprise one or more power management electronic circuitry layers electrically coupled to the cathode and the anode.The management electronic circuitry layers may be formed on a first substrate and a microbattery stack comprising the Li-free cathode, the anode, and the electrolyte film are formed on a second substrate, and wherein the first and second substrates are bonded to each other on respective tops surfaces thereof. The power management electronic circuitry layers and a microbattery stack comprising the Li-free cathode, the anode, and the electrolyte film may be formed on the same substrate. The electronic circuitry layers and the microbattery stack may be formed on the same side of the substrate. The electronic circuitry layers and the microbattery stack are formed on opposite sides of the substrate. The Li-ion thin film microbattery may comprise current collection contacts for the Li-free cathode and the anode, respectively, arranged at the same level.

[0114] In one embodiment, a microbattery array comprising two or more of the Li-ion thin film microbattery of the above described embodiment is provided.

[0115] Figure 18 shows a flow chart 1800 illustrating a method of fabricating a Li-ion thin film microbattery, according to an example embodiment. At step 1802, a Li-free cathode comprising a transition metal oxide thin film is provided. At step 1804, an anode comprising a lithiated Ge or Si thin film is provided. At step 1806, an electrolyte film is disposed between the cathode and the anode, wherein a Li-source of the Li-ion thin film microbattery is provided by means of the lithiated Ge or Si thin film.

[0116] The transition metal oxide may comprise V_2O_5, CrO_3, and/or RuO_2. The electrolyte film may comprise LiPON. The method may further comprise providing one or more power management electronic circuitry layers electrically coupled to the cathode and

the anode. The power management electronic circuitry layers may be formed on a first substrate and a microbattery stack comprising the Li-free cathode, the anode, and the electrolyte film are formed on a second substrate, and wherein the first and second substrates are bonded to each other on respective tops surfaces thereof. The method may comprise forming the power management electronic circuitry layers and a microbattery stack comprising the Li-free cathode, the anode, and the electrolyte film on the same substrate. The method may comprise forming the electronic circuitry layers and the microbattery stack on the same side of the substrate. The method may comprise forming the electronic circuitry layers and the microbattery stack on opposite sides of the substrate. The method may comprise arranging current collection contacts for the Li-free cathode and the anode, respectively, at the same level. Providing the anode may comprise a bi-layer deposition of the semiconductor material and Li, respectively, and controlling a reaction between the semiconductor material and the Li for the lithiation. Providing the anode may comprise a multi-layer deposition of multiple layers of the semiconductor material and Li, respectively, and controlling a reaction between the semiconductor material and the Li for the lithiation. Providing the anode may comprise a co-deposition of the semiconductor material and Li for the lithiation.

[0117] In one embodiment, a method of fabricating a microbattery array is provided, comprising fabricating two or more Li-ion thin film microbatteries using the method of fabricating a Li-ion thin film microbattery of the above embodiment.

[0118] It will be appreciated by a person skilled in the art that numerous variations and/or modifications may be made to the present invention as shown in the specific embodiments without departing from the spirit or scope of the invention as broadly described. The present embodiments are, therefore, to be considered in all respects to be illustrative and not restrictive. Also, the invention includes any combination of features, in particular any combination of features in the patent claims, even if the feature or combination of features is not explicitly specified in the patent claims or the present embodiments.

References

[1] J. M. Kahn, R. H. Katz and K. S. J. Pister, Proceedings of the 5th Annual ACM/IEEE International Conference on Mobile Computing and Networking (1999), p. 271.

[2] F. Vullum and D. Teeters, J. Power Sources, 146, 804 (2005).

[3] N. J. Dudney, Electrochem. Soc. Interface, 17, 44 (2008).

[4] K. S. Park, Y. J. Park, M. K. Kim, J. T. Son, H. G. Kim and S. J. Kim, J. Power Sources, 103, 67 (2001).

[5] X. He, IDTechEx (2015).

[6] W. C. West, J. F. Withacre, V. White and B. V. Ratnakumar, J. Micromech. Microeng., 12, 58 (2002).

[7] J. B. Bates, N. J. Dudney, B. Neudecker, A. Ueda and C. D. Evans, Solid State Ionics, 135, 33 (2000).

[8] N. J. Dudney, Mat. Sci. Eng. B, 106, 245 (2005).

[9] C. M. Haynes, X. Zhao and H. H. Kung, Annual Review of Chemical and Biomolecular Engineering, 3, 445 (2012).

[10] B. A. Boukamp, G. C. Lesh and R. A. Huggins, J. Electrochem. Soc., 128, 725 (1981).

[11] A. Al-Obeidi, D. Kramer, C. V. Thompson and R. Monig, J. Power Sources, 297, 472 (2015).

[12] X. L. Wu, Y. G. Guo and L. J. Wan, Chem. Asian J., 8, 1948 (2013).

[13] J. Graetz, C. C. Ahn, R. Yazami and B. Fulda, J. Elec. Soc., 151, A698 (2004).

[14] R. S. Omampuliyur, M. Bhuiyan, Z. Han, Z. Jing, L. Li, E. A. Fitzgerald, C. V. Thompson and W. K. Choi, J. Nanoscience and Nanotechnology, 15, 4926 (2015).

[15] B. Lafarge, L. L. Jodin, R. Salot and A. Billard, J. Elec. Soc., 155, A181 (2008).

[16] J. Murota, M. Kato, R. Kricher and S. Ono, Journal de Physique IV, 2, C2-795 (1991).

[17] Q. Huang, S. W. Bedell, K. L. Sanger, M. Copel, H. Delizianti and L. T. Romankiw, Electrochem. Solid-State Lett., 10, D124 (2007).

[18] E. Krikorian and R. J. Sneed, J. Applied Physics, 37, 3665 (1996).

[19] Y. J. Park, J. G. Kim, M. K. Kim, H. Y. Chung, W. S. Um, M. H. Kim and H. G. Kim, J. Power Sources, 16, 41 (1998).

[20] A. Mantoux, H. Groulx, E. Balnois, P. Doppelt and L. Gueroudji, J. Electrochem. Soc., 151, A368 (2004).

[21] E. Poitron, A. Le Gal La Salle, A. Verbaere, Y. Piffard and D. Guyomard, Electrochemica Acta, 45, 197 (1999).

[22] R. B. Hadjean, V. Golabkan, J. P. Pereira-Ramos, A. Mantoux and D. Lincot, J. Raman. Spec., 33, 631 (2002).
[23] K. Mitani and U. M. Gosele, J. Electronic Mat., 21, 669 (1992(.

[24] M. A. Schmidt, Proc. of the IEEE, 86, 1575 (1998).

[25] G. Taraschi, A. J. Pitera and E. A. Fitzgerald, Solid-state Electronics, 48, 1297 (2014).

[26] J. B. Bates, N. J. Dudney, B. J. Neudecker, F. X. Hart, H. P. Jun and S. A. Hackney, J. Elec. Soc., 147, 59 (2000).

[27] D. Safaname, D. Damiano, R. P. Rao and S. Adams, Solid State Ionics, 262, 211 (2014).

[28] N. Liu, L. Hu, M. T. McDowell, A. Jackson and Y. Cui, ACS Nano, 5, 6487 (2011).

[29] Y. Kim, S. Muhammad, H. Kim, Y. H. Cho, H. Kim, J. M. Kim, W. S. Yoon, Chem. Sus. Chem. 8 (2015) 2378-2384.

[30] P. Balaya, H. Li, L. Kienle, J. Maier, Adv. Func. Mat. 13 (2003) 621-625.

[31] A. S. Hassan, K. Moyer, B. R. Ramachandran, C. D. Wick, J. Phys. Chem. C 120 (2016) 2036-2046.

[32] J. Zhu, K. B. Yeap, K. Zeng, L. Li, Thin Solid Films 519 (2011) 1914-1922.

[33] J. Zhu, K. Zeng, L. Li, Metallurgical and Materials Transaction A 44A (2013) S26-S34.

[34] C. Shi, B. Walker, E. Zeisel, B. Hu, G. McAllister, IEEE J. Solid-State Circuits 42 (2007) 1723-1731.

[35] Y. Nakase, S. Kirose, H. Onoda, Y. Ido, Y. Shimizu, T. Oishi, T. Kumamoto, T. Shimizu, IEEE J. Solid-State Circuits 48 (2013) 1933-1942.

[36] D. El-Damak, A. Chandrakasan, IEEE J. Solid-State Circuits 51 (2016) 943-954.

[37] S. Ahsnuzzaman, A. Prodic, D. Johns, IEEE J. Solid-State Circuits 31 (2016) 4305-4323.

CLAIMS

What is claimed is:

1. A Li-ion thin film microbattery comprising:
a Li-free cathode comprising a transition metal oxide thin film;
an anode comprising a lithiated Ge or Si thin film; and
an electrolyte film disposed between the cathode and the anode;
wherein a Li-source of the Li-ion thin film microbattery is provided by means of the lithiated Ge or Si thin film.

2. The Li-ion thin film microbattery of claim 1, wherein the transition metal oxide comprises V_2O_5, CrO_3, and/or RuO_2.

3. The Li-ion thin film microbattery of claims 1 or 2, wherein the electrolyte film comprises LiPON.

4. The Li-ion thin film microbattery of any one of claims 1 to 3, further comprising one or more power management electronic circuitry layers electrically coupled to the cathode and the anode.

5. The Li-ion thin film microbattery of claim 4, wherein the power management electronic circuitry layers are formed on a first substrate and a microbattery stack comprising the Li-free cathode, the anode, and the electrolyte film are formed on a second substrate, and wherein the first and second substrates are bonded to each other on respective tops surfaces thereof.

6. The Li-ion thin film microbattery of claim 4, wherein the power management electronic circuitry layers and a microbattery stack comprising the Li-free cathode, the anode, and the electrolyte film are formed on the same substrate.

7. The Li-ion thin film microbattery of claim 6, wherein the electronic circuitry layers and the microbattery stack are formed on the same side of the substrate.

8. The Li-ion thin film microbattery of claim 6, wherein the electronic circuitry layers and the microbattery stack are formed on opposite sides of the substrate.

9. The Li-ion thin film microbattery of any one of claims 1 to 8, comprising current collection contacts for the Li-free cathode and the anode, respectively, arranged at the same level.

10. A microbattery array comprising two or more of the Li-ion thin film microbattery of any one of claims 1 to 9.

11. A method of fabricating a Li-ion thin film microbattery, comprising the steps of:
providing a Li-free cathode comprising a transition metal oxide thin film;
providing an anode comprising a lithiated Ge or Si thin film; and
providing an electrolyte film disposed between the cathode and the anode;
wherein a Li-source of the Li-ion thin film microbattery is provided by means of the lithiated Ge or Si thin film.

12. The method of claim 11, wherein the transition metal oxide comprises V_2O_5, CrO_3, and/or RuO_2.

13. The method of claims 11 or 12, wherein the electrolyte film comprises LiPON.

14. The method of any one of claims 11 to 13, further comprising providing one or more power management electronic circuitry layers electrically coupled to the cathode and the anode.

15. The method of claim 14, wherein the power management electronic circuitry layers are formed on a first substrate and a microbattery stack comprising the Li-free cathode, the anode, and the electrolyte film are formed on a second substrate, and wherein the first and second substrates are bonded to each other on respective tops surfaces thereof.

16. The method of claim 14, comprising forming the power management electronic circuitry layers and a microbattery stack comprising the Li-free cathode, the anode, and the electrolyte film on the same substrate.

17. The method of claim 16, comprising forming the electronic circuitry layers and the microbattery stack on the same side of the substrate.

18. The method of claim 16, comprising forming the electronic circuitry layers and the microbattery stack on opposite sides of the substrate.

19. The method of any one of claims 11 to 18, comprising arranging current collection contacts for the Li-free cathode and the anode, respectively, at the same level.

20. The method of any one of claims 11 to 19, wherein providing the anode comprises a bi-layer deposition of the semiconductor material and Li, respectively, and controlling a reaction between the semiconductor material and the Li for the lithiation.

21. The method of any one of claims 11 to 19, wherein providing the anode comprises a multi-layer deposition of multiple layers of the semiconductor material and Li, respectively, and controlling a reaction between the semiconductor material and the Li for the lithiation.

22. The method of any one of claims 11 to 19, wherein providing the anode comprises a co-deposition of the semiconductor material and Li for the lithiation.

23. A method of fabricating a microbattery array, comprising fabricating two or more Li-ion thin film microbatteries using the method of any one of claims 11 to 22.

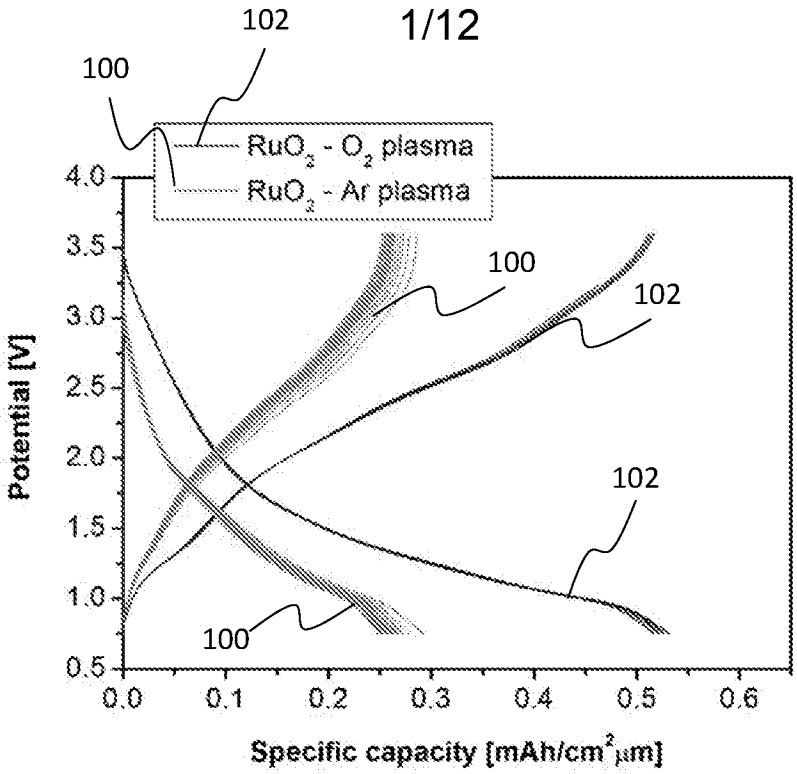


Figure 1

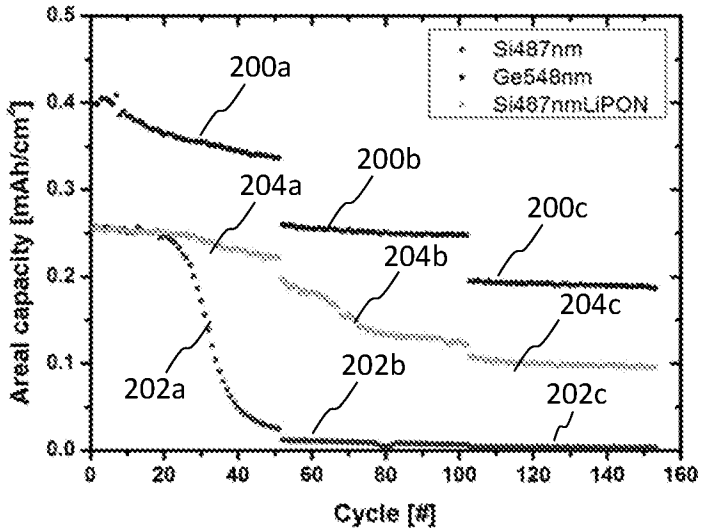


Figure 2

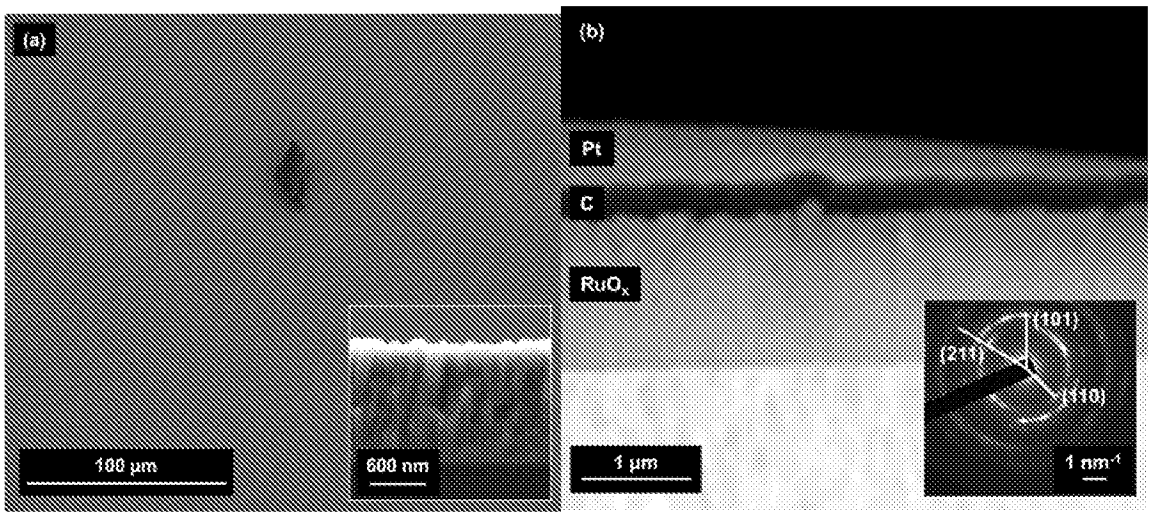


Figure 3

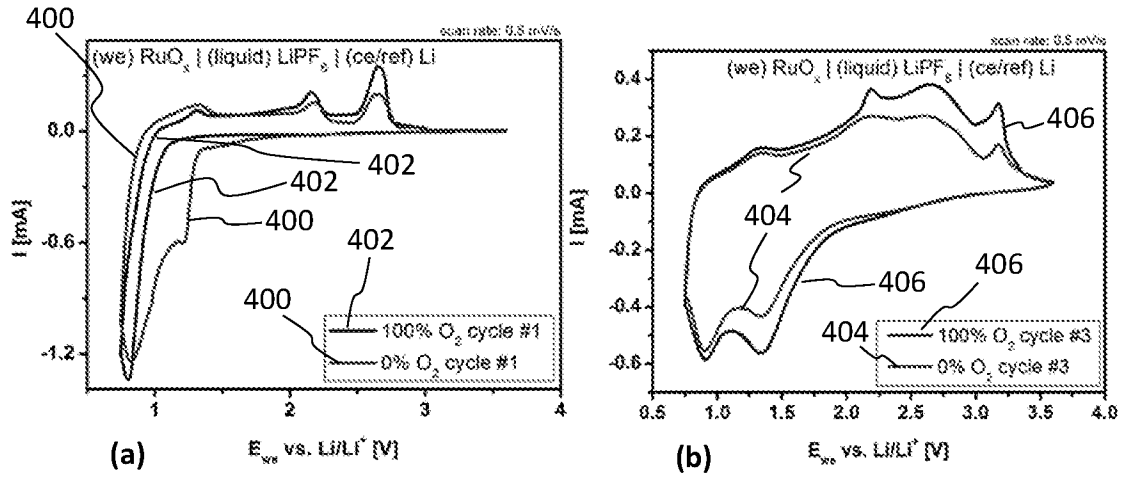


Figure 4

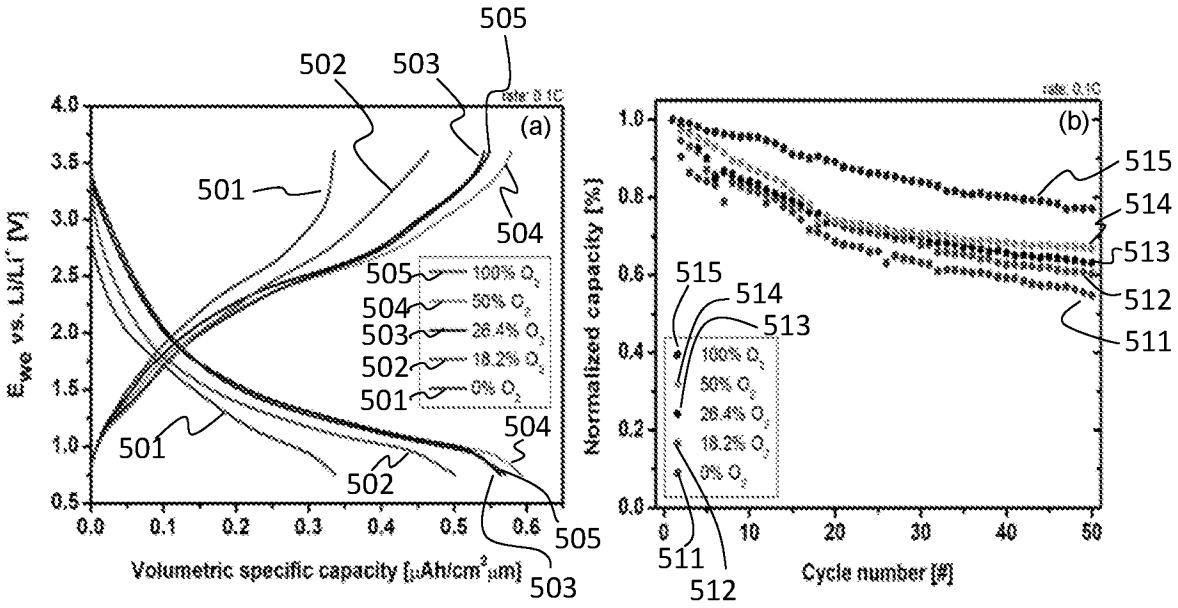


Figure 5

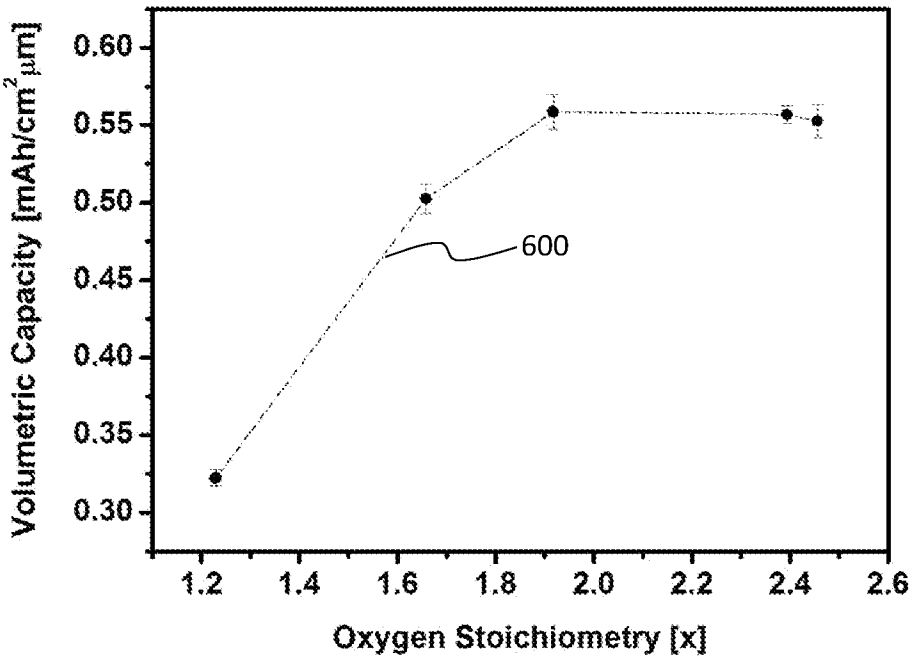


Figure 6

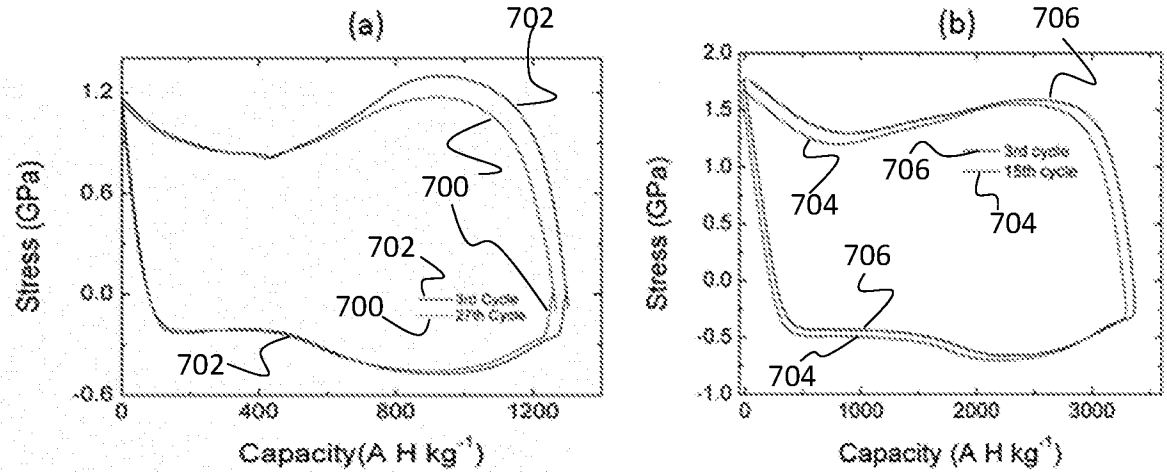


Figure 7

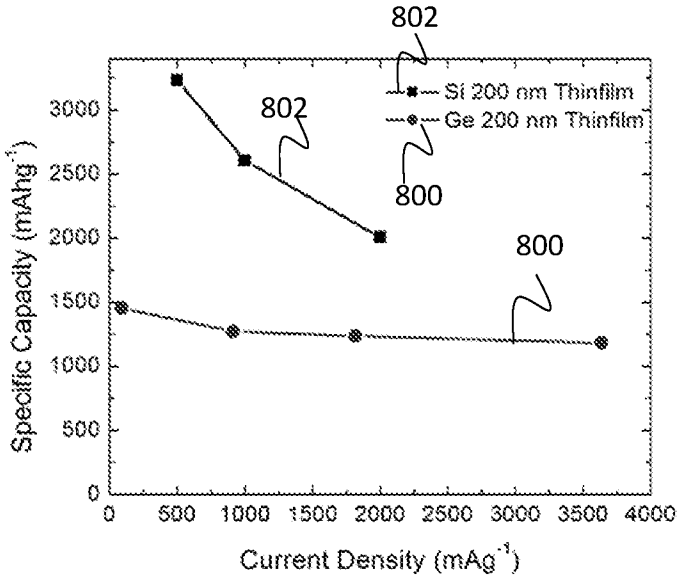


Figure 8

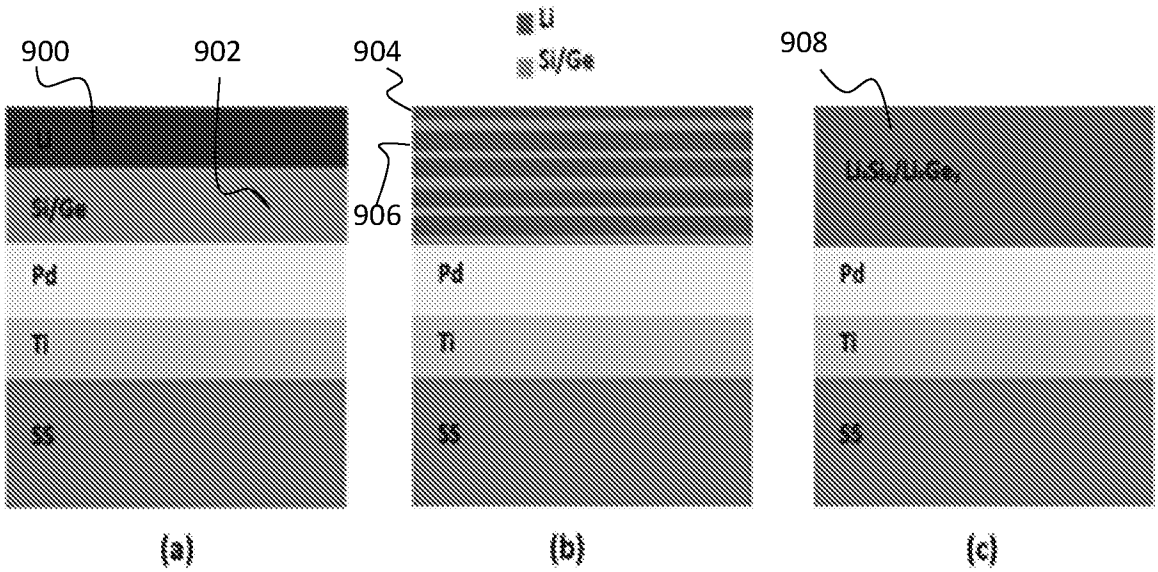


Figure 9

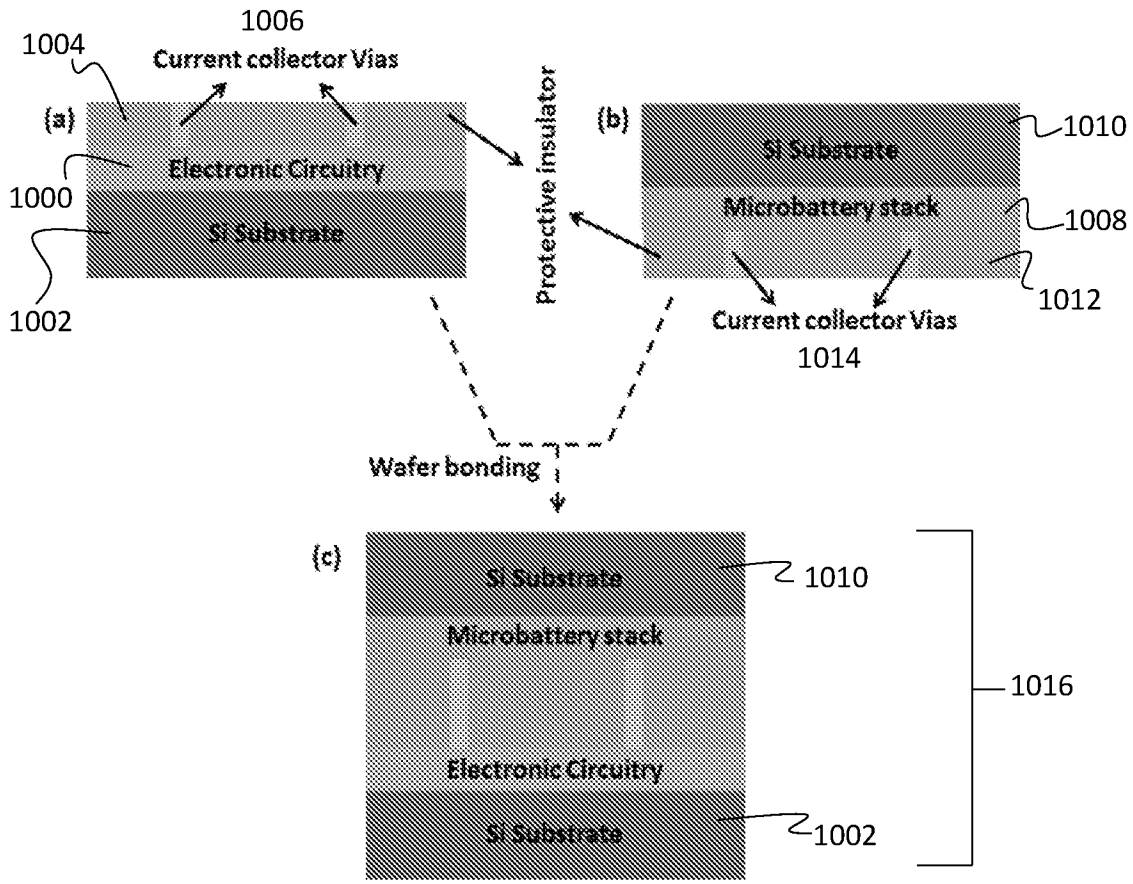


Figure 10

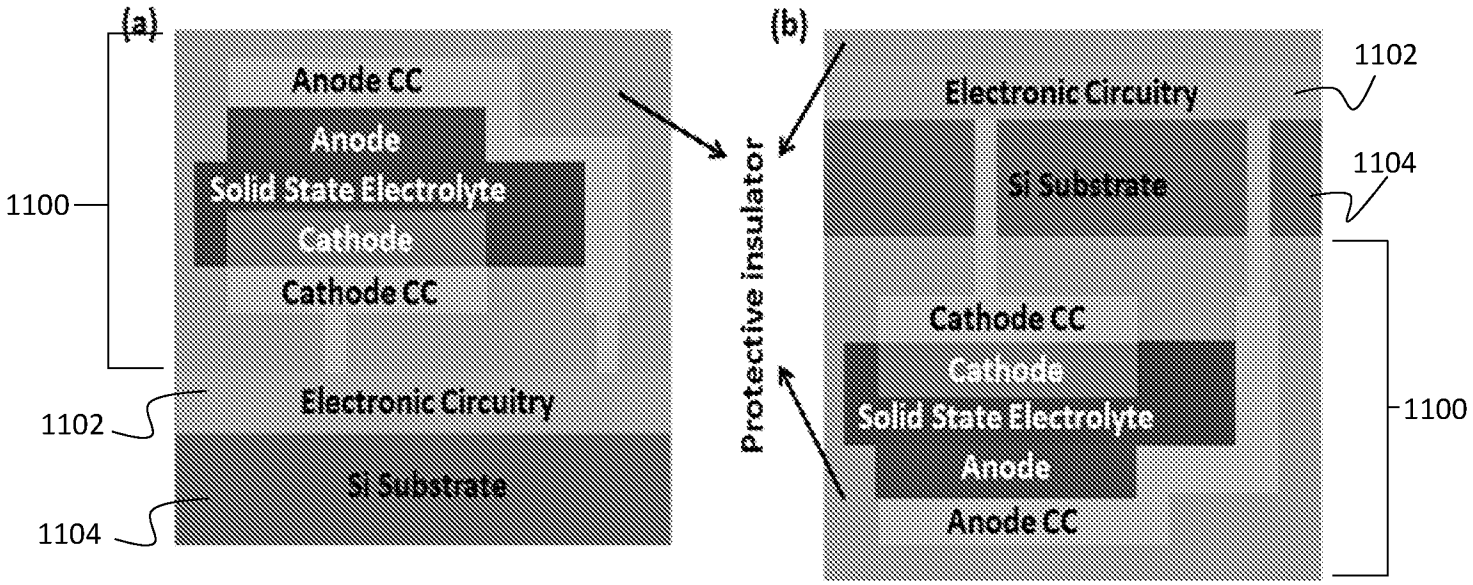


Figure 11

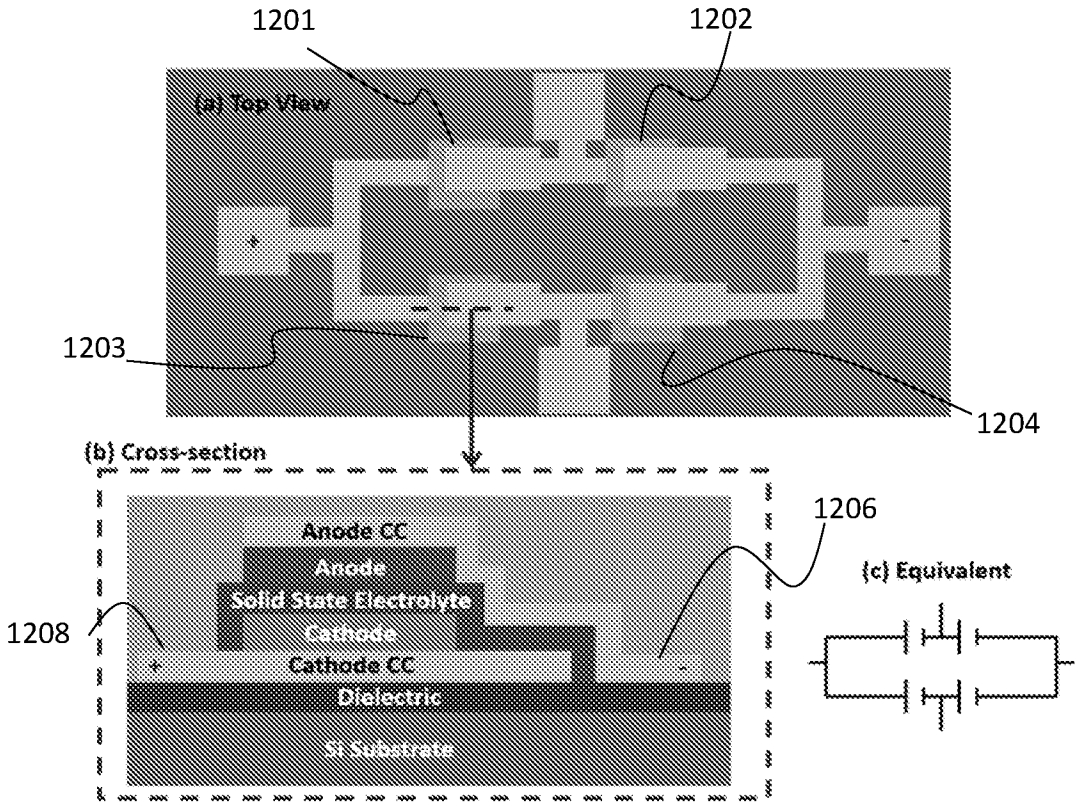


Figure 12

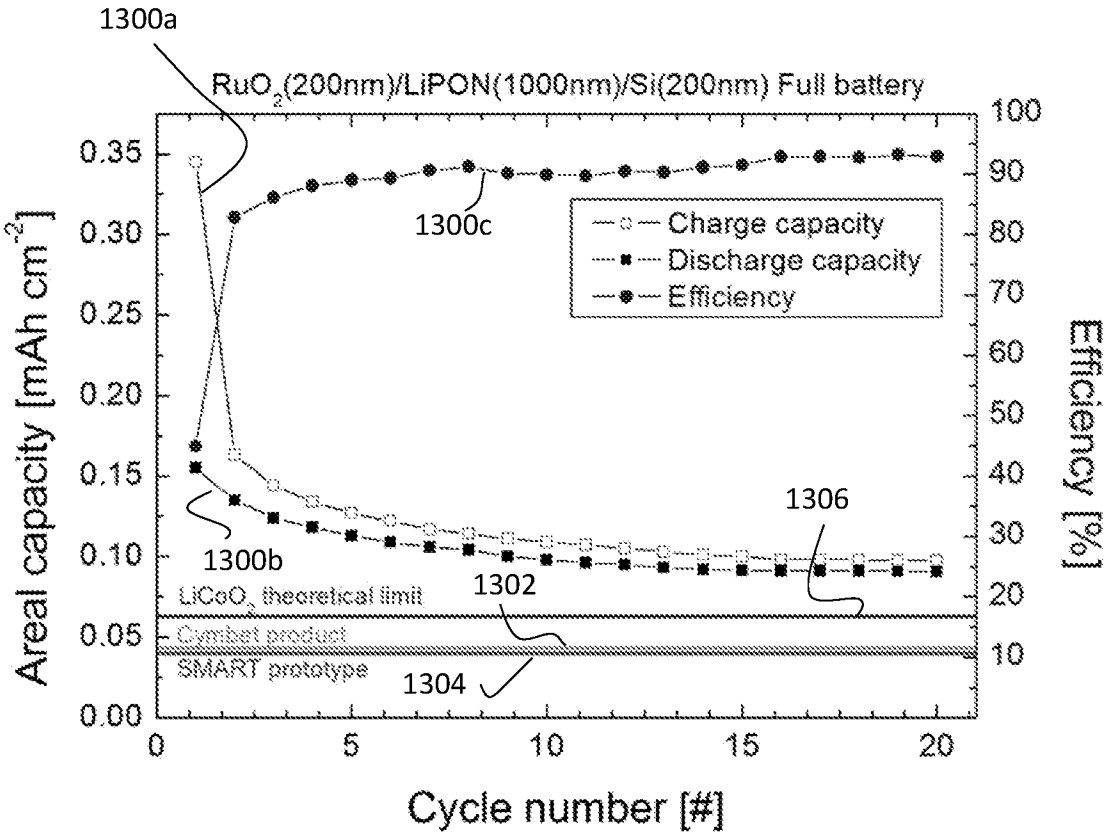
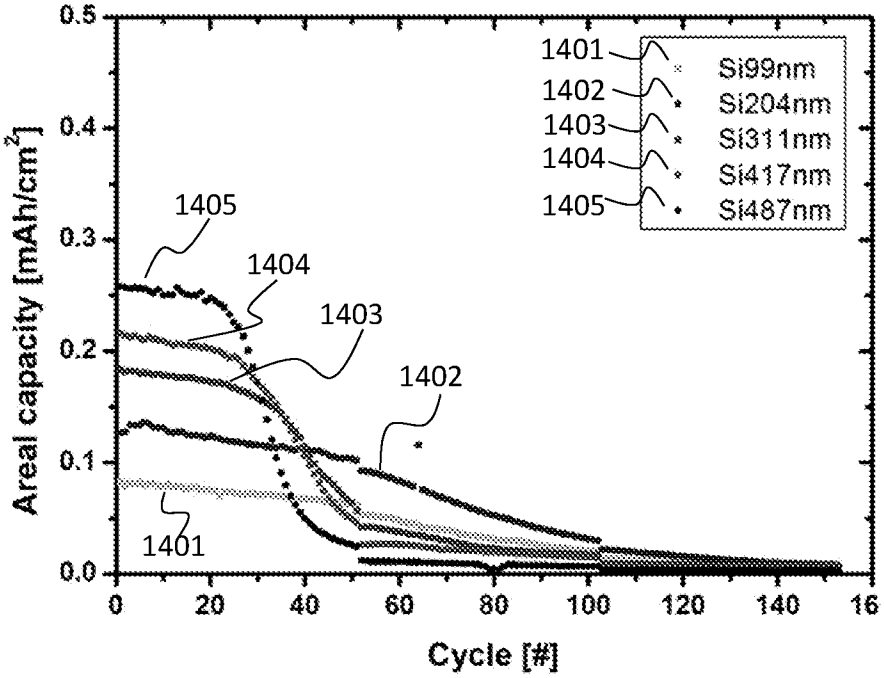
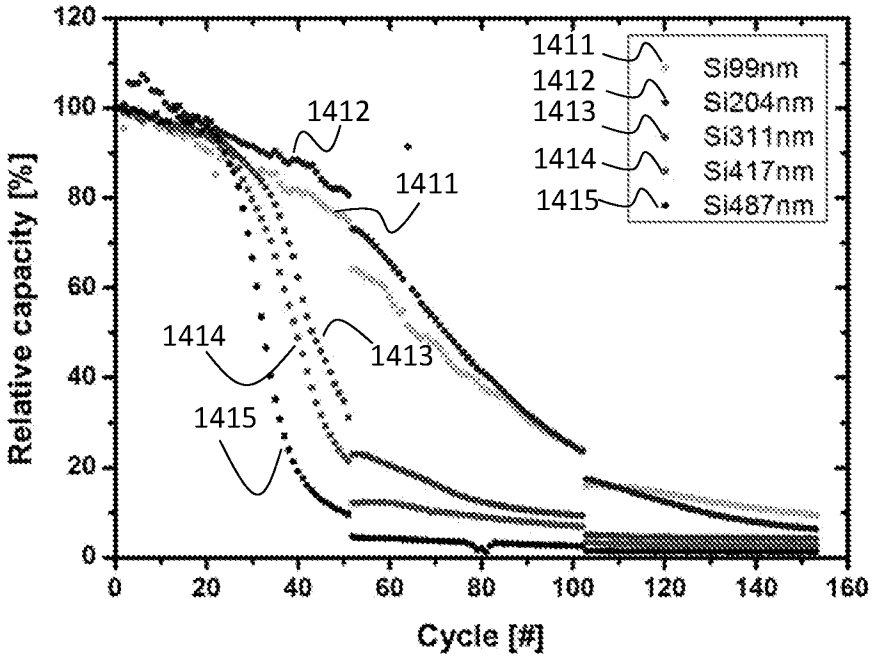

1300a
RuO2(200nm)/LiPON(1000nm)/Si(200nm) Full battery
1300c
Charge capacity
Discharge capacity
Efficiency
1306
1300b
1302
LiCoO2 theoretical limit
Cymbet product
SMART prototype
1304
Areal capacity [mAh cm-2]
Efficiency [%]
Cycle number [#]
0.00
0.05
0.10
0.15
0.20
0.25
0.30
0.35
0
5
10
15
20
10
20
30
40
50
60
70
80
90
100

Figure 13

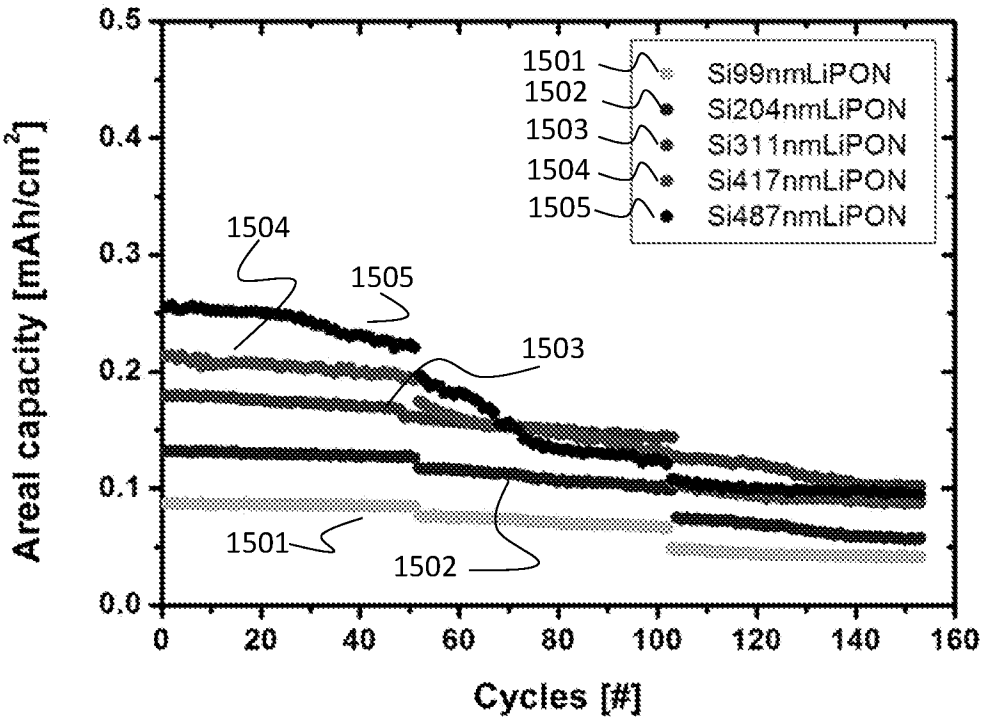

Areal capacity [mAh/cm^2]
Cycle [#]
1401 Si99nm
1402 Si204nm
1403 Si311nm
1404 Si417nm
1405 Si487nm
1405
1404
1403
1402
1401

(a)

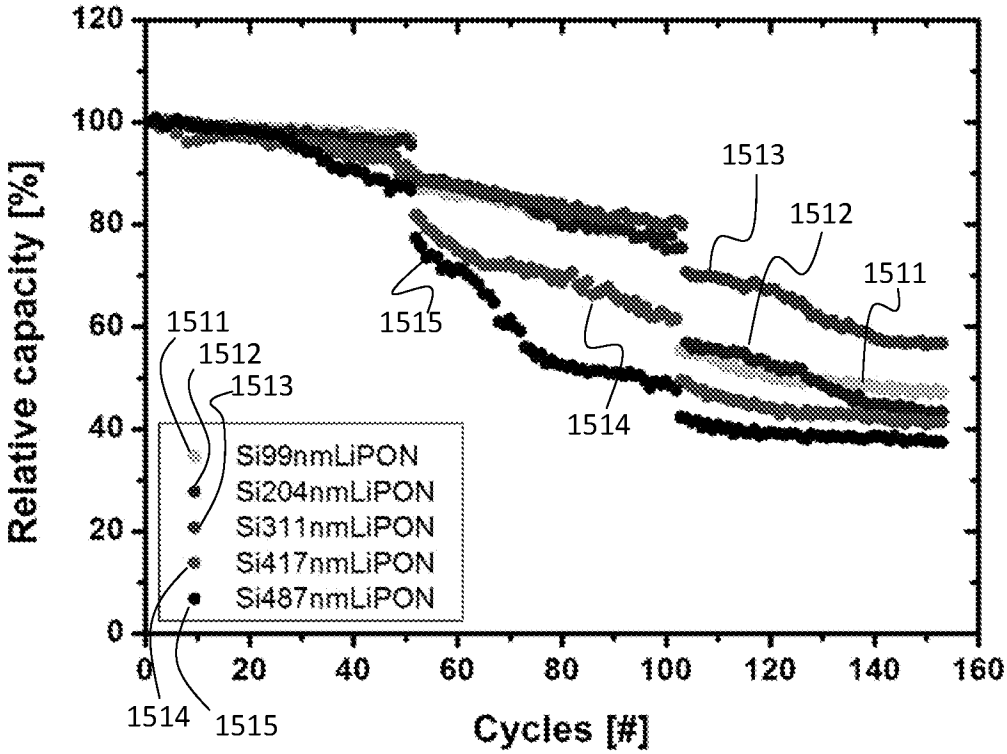

Relative capacity [%]
Cycle [#]
1411 Si99nm
1412 Si204nm
1413 Si311nm
1414 Si417nm
1415 Si487nm
1412
1411
1414
1413
1415

(b)

Figure 14

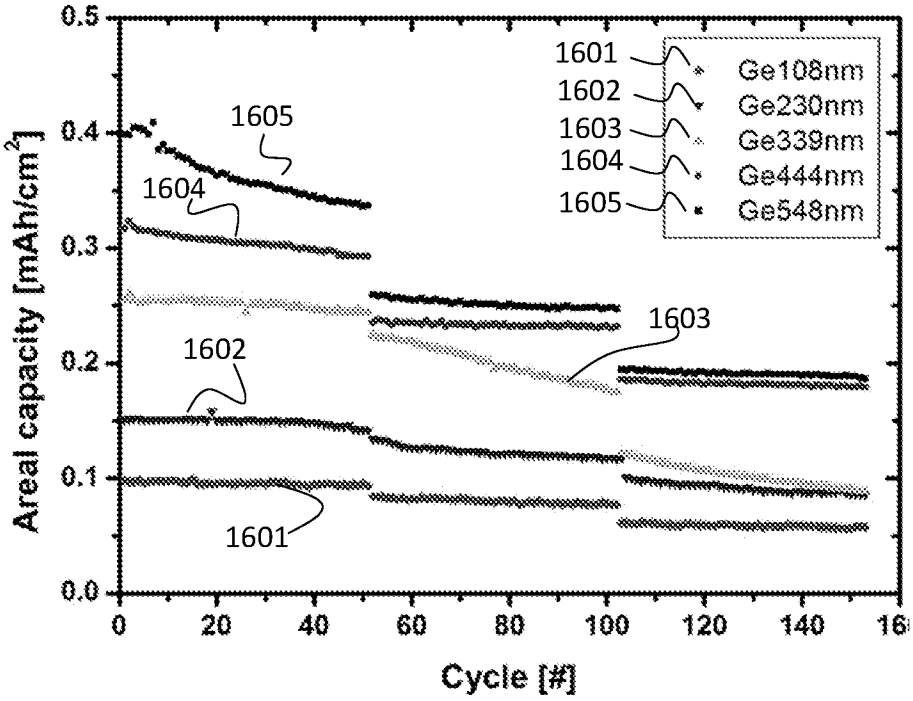

Areal capacity [mAh/cm^2]
Cycles [#]
1501 Si99nmLiPON
1502 Si204nmLiPON
1503 Si311nmLiPON
1504 Si417nmLiPON
1505 Si487nmLiPON
1504
1505
1503
1501
1502

(a)

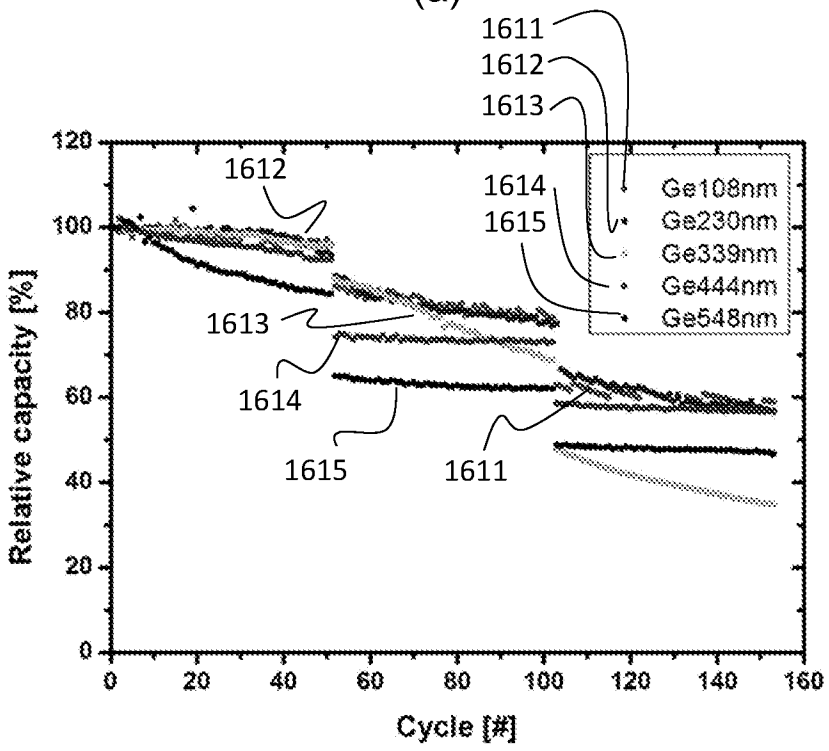

Relative capacity [%]
Cycles [#]
1513
1512
1511
1515
1514
1511
1512
1513
Si99nmLiPON
Si204nmLiPON
Si311nmLiPON
Si417nmLiPON
Si487nmLiPON
1514
1515

(b)

Figure 15

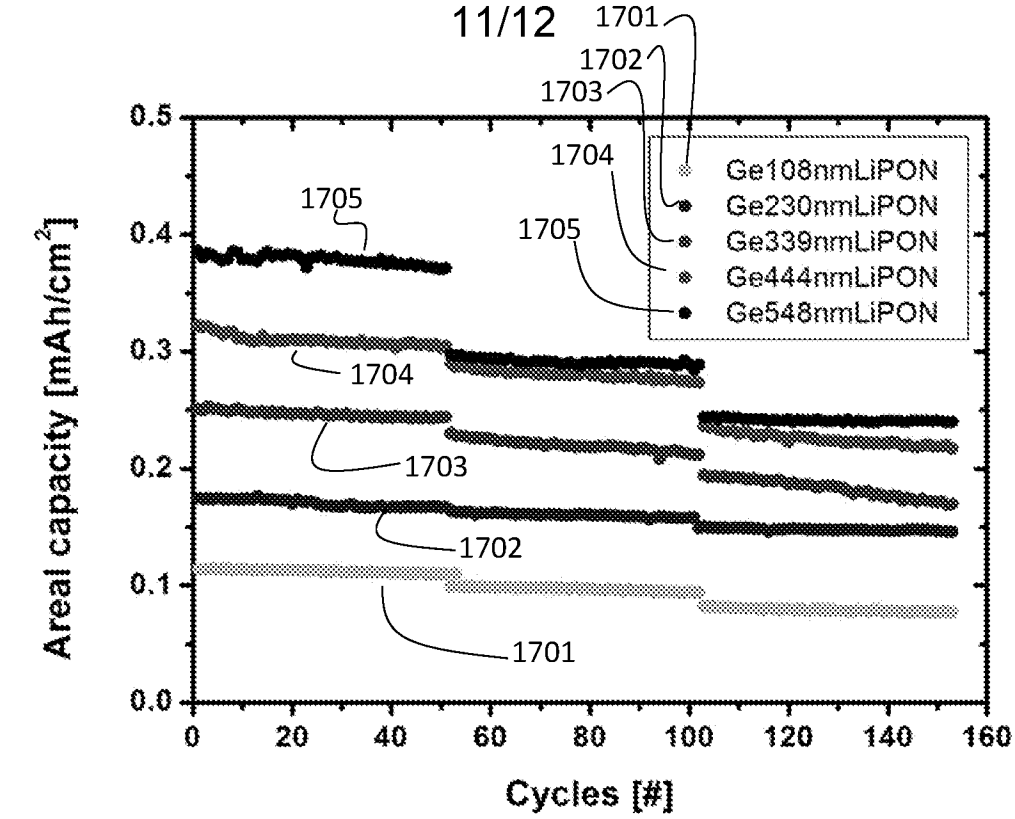

Areal capacity [mAh/cm^2]
Cycle [#]
1601
1602
1603
1604
1605
Ge108nm
Ge230nm
Ge339nm
Ge444nm
Ge548nm

(a)

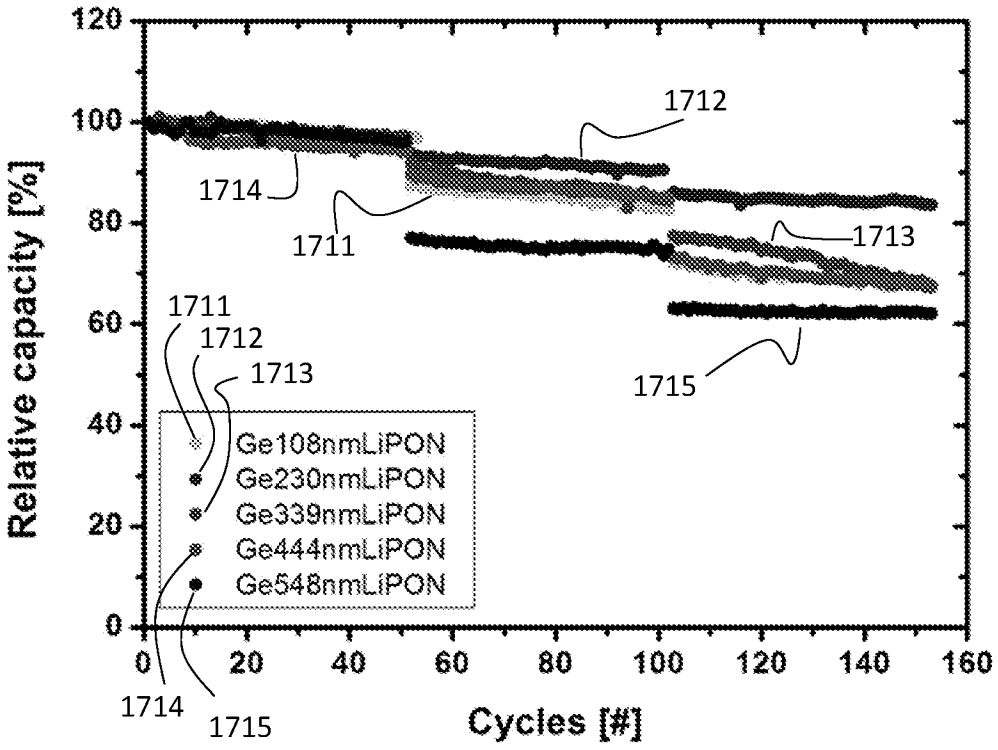

Relative capacity [%]
Cycle [#]
1611
1612
1613
1614
1615
Ge108nm
Ge230nm
Ge339nm
Ge444nm
Ge548nm

(b)

Figure 16

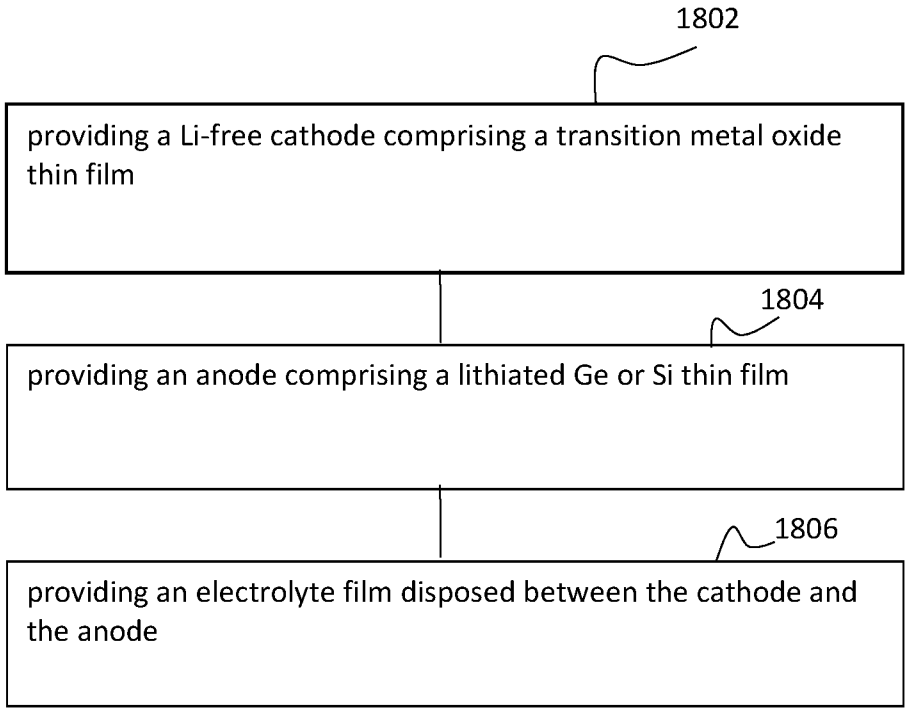

1701
1702
1703
1704
1705
1705
Ge108nmLiPON
Ge230nmLiPON
Ge339nmLiPON
Ge444nmLiPON
Ge548nmLiPON
1704
1703
1702
1701
Areal capacity [mAh/cm^2]
Cycles [#]
0.0
0.1
0.2
0.3
0.4
0.5
0
20
40
60
80
100
120
140
160

(a)


1712
1714
1711
1713
1715
1711
1712
1713
Ge108nmLiPON
Ge230nmLiPON
Ge339nmLiPON
Ge444nmLiPON
Ge548nmLiPON
1714
1715
Relative capacity [%]
Cycles [#]
0
20
40
60
80
100
120
0
20
40
60
80
100
120
140
160

(b)

Figure 17



1800

Figure 18

INTERNATIONAL SEARCH REPORT

International application No.
PCT/US 17/44351

A. CLASSIFICATION OF SUBJECT MATTER

IPC(8) - H01M 4/36, H01M 4/42, H01M 4/02, H01M 4/44, H01M 4/58, H01M 4/38, H01M 4/48 (2017.01)
CPC - H01M 4/38, H01M 2004/021, H01M 10/0525, H01M 4/626, H01M 4/625, H01M 4/587, H01M 4/366, H01M 4/364, H01M 4/134

According to International Patent Classification (IPC) or to both national classification and IPC

B. FIELDS SEARCHED

Minimum documentation searched (classification system followed by classification symbols)

See Search History Document

Documentation searched other than minimum documentation to the extent that such documents are included in the fields searched

See Search History Document

Electronic data base consulted during the international search (name of data base and, where practicable, search terms used)

See Search History Document

C. DOCUMENTS CONSIDERED TO BE RELEVANT

Category*	Citation of document, with indication, where appropriate, of the relevant passages	Relevant to claim No.
Y	US 2010/0173198 A1 (ZAHMU et al.) 08 July 2010 (08.07.2010), para [0085], [0086], [0094], [0106], [0108], [0111], [0112], [0117]	1-3, 11-13
Y	US 2013/0045427 A1 (ZAHMU et al.) 21 February 2013 (21.02.2013), para [0049], [0106], [0113]	1-3, 11-13
Y	US 2007/0015061 A1 (KLAASSEN) 18 January 2007 (18.01.2007), para [0002], [0040]-[0042]	1-3, 11-13
A	US 2014/0342249 A1 (HE et al.) 20 November 2014 (20.11.2014), entire document	1-3, 11-13
A	US 2015/0004495 A1 (CUI et al.) 01 January 2015 (01.01.2015), entire document	1-3, 11-13

☐ Further documents are listed in the continuation of Box C. ☐ See patent family annex.

* Special categories of cited documents:

"A" document defining the general state of the art which is not considered to be of particular relevance

"E" earlier application or patent but published on or after the international filing date

"L" document which may throw doubts on priority claim(s) or which is cited to establish the publication date of another citation or other special reason (as specified)

"O" document referring to an oral disclosure, use, exhibition or other means

"P" document published prior to the international filing date but later than the priority date claimed

"T" later document published after the international filing date or priority date and not in conflict with the application but cited to understand the principle or theory underlying the invention

"X" document of particular relevance; the claimed invention cannot be considered novel or cannot be considered to involve an inventive step when the document is taken alone

"Y" document of particular relevance; the claimed invention cannot be considered to involve an inventive step when the document is combined with one or more other such documents, such combination being obvious to a person skilled in the art

"&" document member of the same patent family

Date of the actual completion of the international search	Date of mailing of the international search report
21 September 2017	23 OCT 2017
Name and mailing address of the ISA/US Mail Stop PCT, Attn: ISA/US, Commissioner for Patents P.O. Box 1450, Alexandria, Virginia 22313-1450 Facsimile No. 571-273-8300	Authorized officer: Lee W. Young PCT Helpdesk: 571-272-4300 PCT OSP: 571-272-7774

Form PCT/ISA/210 (second sheet) (January 2015)

INTERNATIONAL SEARCH REPORT

International application No.
PCT/US 17/44351

Box No. II Observations where certain claims were found unsearchable (Continuation of item 2 of first sheet)

This international search report has not been established in respect of certain claims under Article 17(2)(a) for the following reasons:

1. ☐ Claims Nos.:
because they relate to subject matter not required to be searched by this Authority, namely:

2. ☐ Claims Nos.:
because they relate to parts of the international application that do not comply with the prescribed requirements to such an extent that no meaningful international search can be carried out, specifically:

3. ☒ Claims Nos.: 4-10, 14-23
because they are dependent claims and are not drafted in accordance with the second and third sentences of Rule 6.4(a).

Box No. III Observations where unity of invention is lacking (Continuation of item 3 of first sheet)

This International Searching Authority found multiple inventions in this international application, as follows:

1. ☐ As all required additional search fees were timely paid by the applicant, this international search report covers all searchable claims.

2. ☐ As all searchable claims could be searched without effort justifying additional fees, this Authority did not invite payment of additional fees.

3. ☐ As only some of the required additional search fees were timely paid by the applicant, this international search report covers only those claims for which fees were paid, specifically claims Nos.:

4. ☐ No required additional search fees were timely paid by the applicant. Consequently, this international search report is restricted to the invention first mentioned in the claims; it is covered by claims Nos.:

Remark on Protest

☐ The additional search fees were accompanied by the applicant's protest and, where applicable, the payment of a protest fee.

☐ The additional search fees were accompanied by the applicant's protest but the applicable protest fee was not paid within the time limit specified in the invitation.

☐ No protest accompanied the payment of additional search fees.